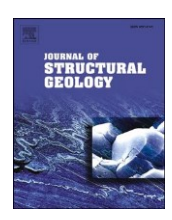
EI SEVIER

Contents lists available at ScienceDirect

Journal of Structural Geology

journal homepage: www.elsevier.com/locate/jsg





Extreme ductile thinning of Cambrian marbles in the Northern Snake Range metamorphic core complex, Nevada, USA: Implications for extension magnitude and structural evolution

Sean P. Long a,*, Jeffrey Lee b, Nolan R. Blackford a,c

- ^a School of the Environment, Washington State University, Pullman, WA, 99164, USA
- ^b Department of Geophysics, Colorado School of Mines, Golden, CO, 80401, USA
- ^c Arizona Geological Survey, Tucson, AZ, 85721, USA

ABSTRACT

The detailed stratigraphy of rocks within the Northern Snake Range metamorphic core complex provides an exceptional opportunity to investigate the geometry and magnitude of ductile strain during high-magnitude continental extension. In the northern part of the range, Middle-Late Cambrian marbles in the footwall of the Northern Snake Range d`ecollement (NSRD), which have a stratigraphic thickness of 1107 ± 107 m in adjacent ranges, were thinned during Late Eocene-Late Oligocene ductile extension. From west to east across the range, these rocks have been thinned from 869-935-m-thick (15–21% structural thinning) to 54-88-m-thick (92–95% structural thinning) across a 12 km lineation-parallel distance. Ductile extensional strain was accompanied by the development of pervasive linear-planar fabrics and produced megaboudins of calcareous schist units that are 100-500-m-long, 15-25-m-thick, and separated by as much as 1 km. The magnitude of lineation-parallel ductile extension increases eastward across the range from $24 \pm 21\%$ to $1226 \pm 256\%$, and total ductile extension across the range is 12.1 ± 2.2 km ($167 \pm 31\%$). Quartz recrystallization microstructures and published calcite-dolomite thermometry indicate deformation temperatures of ~ 400 –550 °C during initial Late Eocene-Late Oligocene ductile extensional shearing. West to east across the range, rocks in the NSRD footwall experienced a progressively longer ductile extensional strain history and a prolonged residence time at higher temperatures, which was aided by the eastward migration of denudation-related cooling and was likely enhanced by strain heating and/or a pre-extensional eastward dip of footwall rocks. These factors promoted the development of the extreme strain gradient.

1. Introduction

Documenting the geometry, magnitude and kinematics of ductile deformation can provide vital insights into the structural and rheological evolution of continental lithosphere during extensional tectonism (e.g., Lee et al., 1987; Malavieille, 1987; Wells and Allmendinger, 1990; Bailey and Eyster, 2003; Jessup et al., 2006; Singleton and Mosher, 2012). Metamorphic core complexes are exceptional field localities for investigating ductile deformation processes that operate at mid-crustal levels (e.g., Crittenden et al., 1980; Lister and Davis, 1989; Platt et al., 2015). Studies of Cenozoic metamorphic core complexes that extended the thick crust of the North American Cordilleran mountain belt have resulted in models for high-magnitude extension (e.g., Wernicke, 1981; Wernicke and Burchfiel, 1982; Davis, 1983; Miller et al., 1983; Coney and Harms, 1984; Buck, 1988; Lister and Davis, 1989; McGrew et al., 2000; Whitney et al., 2013) that have been exported globally to understand extensional tectonics elsewhere (e.g., Lister et al., 1984; Gessner et al., 2001; Morris et al., 2009).

The Northern Snake Range metamorphic core complex in eastcentral Nevada (Fig. 1A) has been a seminal field locality for investigating the style, geometry, magnitude and timing of both brittle and ductile extensional deformation processes (e.g., Coney, 1974; Gans and Miller, 1983; Miller et al., 1983; Gans, 1987; Lee et al., 1987; 2017; Lee and Sutter, 1991; Lee, 1995; Lewis et al., 1999; Cooper et al., 2010A, 2010B; Long, 2019; Wrobel et al., 2021; Hoiland et al., 2022; Long et al., 2022). Geologic mapping of the majority of the Northern Snake Range at 1:24,000-scale (Lee et al., 1999A, 1999B; 1999C; Gans et al., 1999A, 1999B; Miller and Gans, 1999; Miller et al., 1999B; Johnston, 2000) has provided exceptional stratigraphic context for both the hanging wall and footwall of the top-down-to-ESE Northern Snake Range d'ecollement (NSRD), which is the master extensional structure in the range (Fig. 1B). Neoproterozoic-Cambrian metasedimentary rocks in the footwall of the NSRD were ductilely stretched and thinned during Late Eocene-Late Oligocene extension (e.g., Miller et al., 1983; Lee et al., 1987). Undeformed sections of these rocks exposed in adjacent ranges (e.g., Young, 1960; Dechert, 1967; Drewes, 1967; Whitebread, 1969; Rodgers, 1987;

E-mail address: sean.p.long@wsu.edu (S.P. Long).

^{*} Corresponding author.

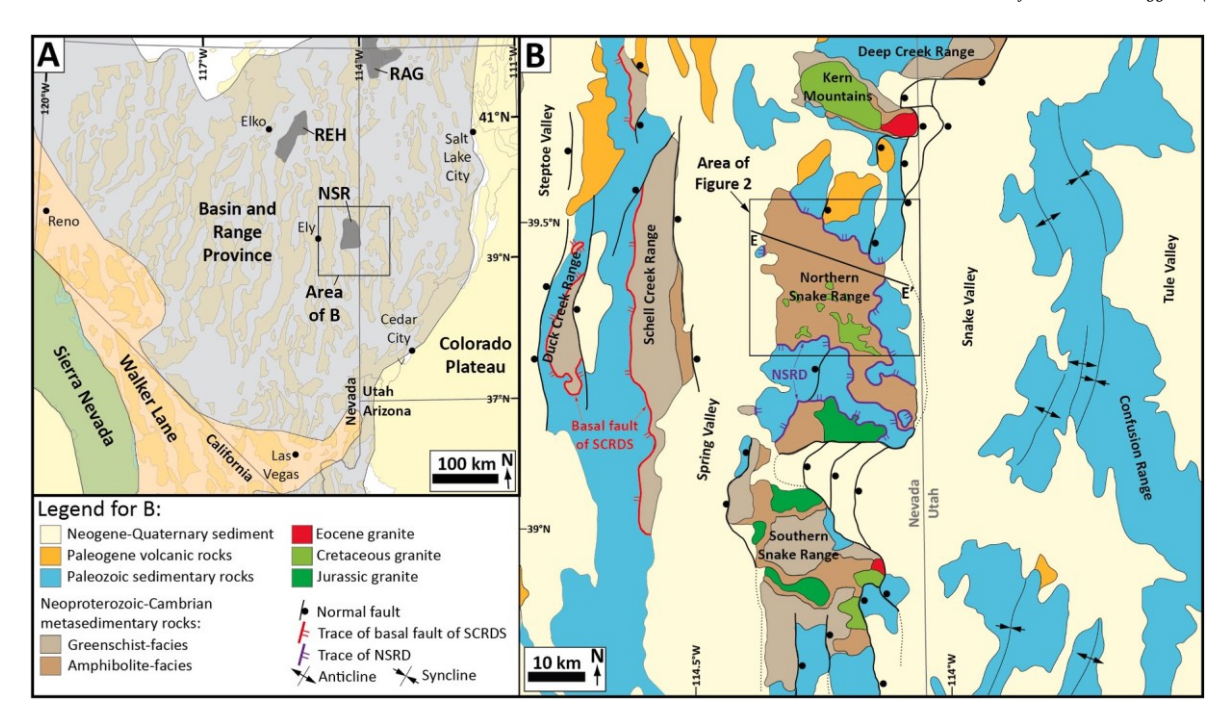


Fig. 1. A) Map of modern tectonic and physiographic provinces in western Utah, Nevada, and southeastern California (modified from Long, 2019), showing the locations of the Northern Snake Range (NSR), Ruby-East Humboldt (REH) and Raft River-Albion-Grouse Creek (RAG) metamorphic core complexes. B) Generalized geologic map of a portion of east-central Nevada and west-central Utah (modified from Lee et al., 2017). The map traces of the Northern Snake Range d'ecollement (NSRD) and the basal fault of the Schell Creek Range detachment system (SCRDS) are shown in purple and red, respectively. (For interpretation of the references to colour in this figure legend, the reader is referred to the Web version of this article.)

Miller et al., 1994) provide stratigraphic markers from which the magnitudes of subvertical ductile thinning and subhorizontal ductile extension can be measured. These methods have been employed in Neoproterozoic-Early Cambrian clastic rocks in the southern part of the range, where estimates of macro-scale ductile thinning have been integrated with finite strain measurements from stretched quartz clasts to define a dramatic increase from 28% ductile thinning at the western flank of the range to 81–94% thinning at the eastern flank (Miller et al., 1983; Lee et al., 1987; Hoiland et al., 2022; Long et al., 2022; Blackford, 2023). In the northern part of the range, five Middle-Late Cambrian, marble-dominated rock units underlie the NSRD, and 1:24,000-scale mapping shows an eastward increase in ductile thinning of the NSRD footwall, similar to that documented in the southern part of the range (Lee et al., 1999A, 1999B; Gans et al., 1999A).

In this study, we quantify the magnitude of Late Eocene-Late Oligocene extensional ductile strain in the footwall of the NSRD in the northern part of the Northern Snake Range by measuring ductile thinning magnitudes within Middle-Late Cambrian marble units. We illustrate the spatial extent of the linear-planar ductile fabrics that were generated by this ductile thinning and document spectacular macroscale boudinage of intervals of calcareous schist within the marble package. Using a range-wide cross section, we generate a model for finite strain in the NSRD footwall across the northern part of the range, which allows us to quantify Late Eocene-Late Oligocene ductile extension and interpret the structural evolution of the footwall of this classic Cordilleran core complex.

2. Tectonic framework of east-central Nevada

Following the \sim 720-660 Ma rifting of the western margin of Laurentia, eastern Nevada (Fig. 1) resided within a passive margin setting in which up to \sim 5–7 km of late Neoproterozoic-Early Cambrian clastic rocks were deposited (e.g., Poole et al., 1992; Yonkee et al., 2014). This was followed by deposition of up to \sim 6–8 km of dominantly shallow-marine carbonates between the Middle Cambrian and Triassic

(e.g., Stewart, 1980).

The consolidation of the western North American margin into an Andean-style subduction zone during the Jurassic initiated the construction of the Cordilleran orogenic belt (e.g., Allmendinger, 1992; Burchfiel et al., 1992; DeCelles, 2004). An eastward-migrating retroarc fold-thrust-belt was constructed across Nevada and western Utah, which culminated in ~150-220 km of shortening in the Sevier fold-thrust belt in western Utah between ~125 and 50 Ma (e.g., Coogan, 1992; DeCelles and Coogan, 2006; Yonkee and Weil, 2015). Eastern Nevada resided in a broad hinterland region to the west of the Sevier fold-thrust belt and experienced diffuse, low-magnitude upper-crustal shortening (~35 km total shortening at ~39°N; Blackford et al., 2022) that was accommodated by thrust faults with km-scale displacement and long-wavelength, open folds (e.g., Gans and Miller, 1983; Taylor et al., 2000; Long, 2012; 2015; Greene, 2014). Localized deep structural burial accommodated by Cordilleran contractional deformation has been interpreted in the vicinity of metamorphic core complexes on the basis of thermobarometry of exhumed metasedimentary rocks (e.g., Camilleri and Chamberlain, 1997; Lewis et al., 1999; McGrew et al., 2000; Cooper et al., 2010B; Hallett and Spear, 2014). However, a lack of evidence for the structures that could have accommodated such deep burial has led to a vigorous debate over this topic (e.g., Henry et al., 2011; Long, 2012; 2015; 2019; Zuza et al., 2020; 2022; Blackford et al., 2022; Wrobel et al., 2021; Hoiland et al., 2022).

During the Late Cretaceous and Paleogene, eastern Nevada is interpreted to have been the site of a ~2.2–3.5 km-elevation orogenic plateau that was underlain by > 50 km-thick crust (e.g., Coney and Harms, 1984; DeCelles, 2004; Cassel et al., 2014; Snell et al., 2014; Chapman et al., 2015; Long, 2019). Contractional deformation migrated eastward into Utah and Colorado during the Paleocene and Eocene, constructing the uplifts of the Laramide province, which has been attributed to shallowing of the subduction angle (e.g., Dickinson and Snyder, 1978). Between the late Eocene and middle Miocene, felsic volcanism of the Great Basin ignimbrite flareup swept southwestward across Nevada (e.g., Best et al., 2009; Henry and John, 2013) and has been attributed to

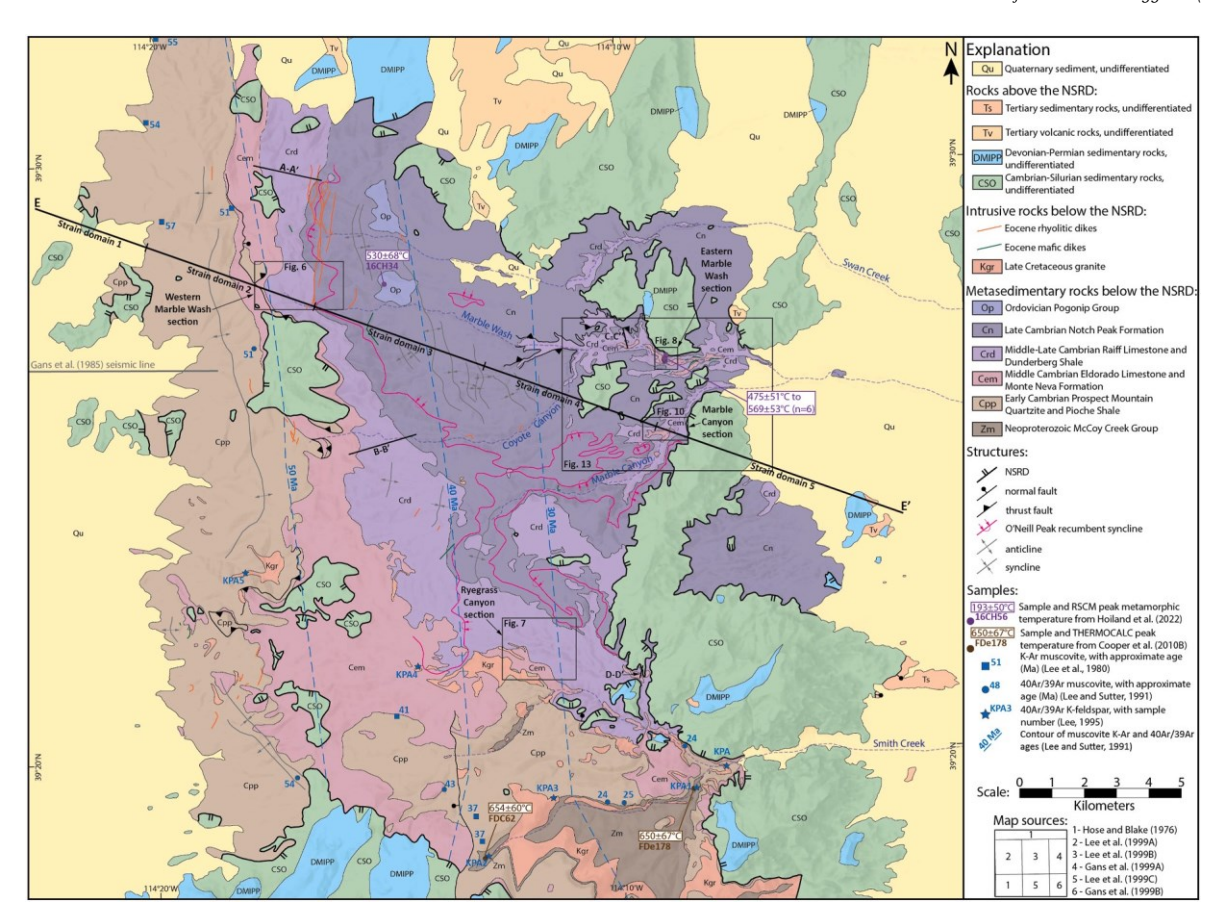


Fig. 2. Geologic map of the northern half of the Northern Snake Range (compiled from Hose and Blake, 1976; Gans et al., 1999A, 1999B; Lee et al., 1999A, 1999B; 1999C). The map trace of the O'Neill Peak recumbent syncline is from Wrobel et al. (2021). The areas of the detailed geologic maps of the Western Marble Wash (Fig. 6), Ryegrass Canyon (Fig. 7), Eastern Marble Wash (Fig. 8) and Marble Canyon (Fig. 10) sections are shown, as well as cross sections A-A', B-B', C-C', and D-D' (see Fig. 11). The section line for cross section E-E' is shown, with the locations of our five strain domains labeled along the section line (see Fig. 15).

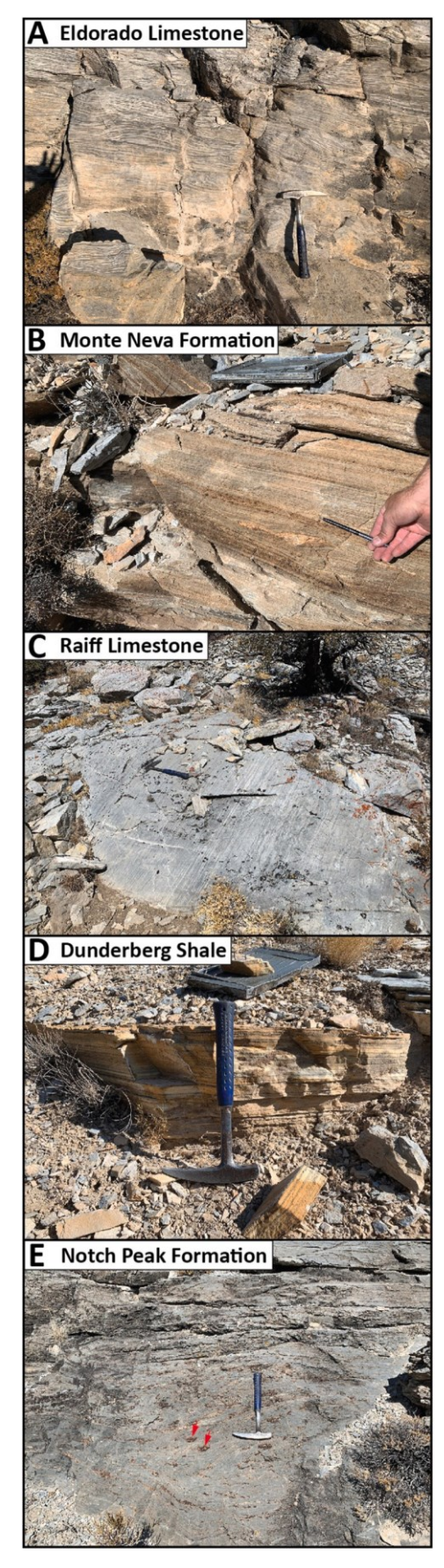
slab rollback (e.g., Humphreys, 1995; Dickinson, 2002). During this time interval (~40-17 Ma), a large region of eastern Nevada and westernmost Utah underwent extension (e.g., Gans and Miller, 1983; Axen et al., 1988; Gans et al., 1989; 2001; Taylor et al., 1989; Druschke et al., 2009; Lee et al., 2017; Long et al., 2018; 2022), which has been interpreted as the initial collapse of the thick crust of the Cordilleran plateau, initiated either by a decrease in interplate coupling accompanying slab rollback (e.g., Dickinson, 2002; Smith et al., 2014; Long et al., 2018) or the influx of magma and related heating and increase in gravitational potential energy during the ignimbrite flareup (e.g., Axen et al., 1993; Humphreys, 1995; Sonder and Jones, 1999; Lund-Snee and Miller, 2022). In east-central Nevada, this extension included normal faulting and ductile stretching in the Northern Snake Range metamorphic core complex (e.g., Miller et al., 1983; Lee et al., 1987; 2017; Gans et al., 1989) and brittle extension in the Schell Creek, Duck Creek and Egan Ranges to the west (Wernicke, 1981; Gans et al., 1989; 2001; Druschke et al., 2009; Long et al., 2022), the Kern Mountains and Deep Creek Range to the north (Rodgers, 1987; Gans et al., 1989), and the Southern Snake Range to the south (e.g., McGrew, 1993; Miller et al., 1999A; Evans et al., 2015) (Fig. 1B).

Eocene-Oligocene extension in east-central Nevada was followed by widespread Neogene high-angle normal faulting that constructed the Basin and Range Province (Fig. 1A) (e.g., Miller et al., 1999A, Dickinson, 2002). Basin and Range-style normal faulting in east-central Nevada locally began as early as ~27 Ma (Anderson et al., 1983), but in most places is constrained by low-temperature thermochronometry to have begun no earlier than ~22-17 Ma (e.g., Lee, 1995; Miller et al., 1999A; Stockli, 1999; Evans et al., 2015).

3. Geologic background of the Northern Snake Range

The Northern Snake Range metamorphic core complex is a highstrain extensional province characterized by the low-dip-angle, topdown-to-ESE NSRD, which has been mapped across the ~30 km eastwest width and ~45 km north-south length of the range (Fig. 1B and 2) (e.g., Gans et al., 1999A, 1999B; Lee et al., 1999A, 1999B; 1999C; Miller et al., 1999B; Miller and Gans, 1999; Johnston, 2000). The NSRD separates a domain of polyphase brittle normal faulting within unmetamorphosed Cambrian to Permian carbonates in its hanging wall from a domain of ductilely stretched, greenschist-to amphibolite-facies, Neoproterozoic-Cambrian metasedimentary rocks in its footwall (e.g., Gans and Miller, 1983; Miller et al., 1983). Rocks in the NSRD footwall exhibit mylonitic, linear-planar ductile fabrics that record subhorizontal stretching and subvertical thinning, with foliations that are subparallel to the NSRD and ESE-trending (110–125° average azimuth range) mineral stretching lineations that demarcate the extension direction (e. g., Miller et al., 1983; Lee et al., 1987). In the southeastern part of the range, mica fish and oblique quartz foliations in the NSRD footwall define a dominant top-down-to-ESE shear sense (Lee et al., 1987). A transition in quartz crystallographic fabrics from symmetric crossed-girdle patterns in the southwestern part of the range to asymmetric, top-down-to-ESE single girdle patterns in the southeastern part has been interpreted to represent an eastward transition from pure shear-dominant to simple shear-dominant extensional ductile shearing in the NSRD footwall (Lee et al., 1987; G'ebelin et al., 2011; 2015).

The NSRD has been gently domed across the east-west width of range, with $\sim 5-15^{\circ}$ dips on the range flanks and a subhorizontal dip at the range crest (e.g., Lee, 1990; Gans et al., 1999A, 1999B; Lee et al.,



(caption on next column)

Fig. 3. Photographs of representative lithologies of the five Middle-Late Cambrian rock units below the NSRD. A) Characteristic striped appearance of alternating light gray and blue-gray laminations in bluff-forming marble of the Eldorado Limestone (Eastern Marble Wash transect). B) Green-brown to tan, micaceous marble interlayer characteristic of the Monte Neva Formation (Marble Canyon transect). C) Bluff-forming marble with closely spaced, lightgray to dark blue-gray laminations characteristic of the Raiff Limestone (Western Marble Wash transect). D) Tan, bluff-forming, micaceous marble interlayer characteristic of the Dunderberg Shale (Eastern Marble Wash transect). E) Bluff-forming, medium-to dark-gray marble with brown chert stringers and nodules (highlighted with red arrows) characteristic of the Notch Peak Formation (Eastern Marble Wash transect). (For interpretation of the references to colour in this figure legend, the reader is referred to the Web version of this article.)

1999C; Miller et al., 1999B; Miller and Gans, 1999). At least 16–36 km of displacement was fed eastward into the NSRD from a brittle breakaway fault system exposed to the west (Fig. 1B) (the Schell Creek Range detachment system; Blackford et al., 2022; Long et al., 2022), and an additional 13–25 km of extension was accommodated by normal faulting above the NSRD in the Northern Snake Range (Miller et al., 1983; Long, 2019; Long et al., 2022).

The NSRD exhibits a footwall flat at the top of the Early Cambrian Prospect Mountain Quartzite across the full ~30 km width of the southern part of the range (Miller et al., 1983; 1999B; Miller and Gans, 1999; Johnston, 2000). Finite strain analyses from stretched quartz clasts and quartzite pebbles in Neoproterozoic-Early Cambrian clastic rocks in the NSRD footwall demonstrate an increase from 30% subhorizontal extension and 28% subvertical thinning at the southwestern flank of the range to at least 450% extension and at least 81% thinning at the southeastern flank (Lee et al., 1987; Long et al., 2022; Blackford, 2023). This strain gradient is corroborated by structural thinning of the Prospect Mountain Quartzite, which has a uniform regional stratigraphic thickness of ~ 1.2 km but thins to as little as $\sim 50-250$ m at the eastern flank of the range, corresponding to ~80-95% ductile thinning (Miller et al., 1983; Lee et al., 1987; Hoiland et al., 2022; Blackford, 2023). These strain and thinning datasets define 19.1–19.7 km of total subhorizontal ductile extension of the NSRD footwall (220-259%) across the southern part of the range (Lee et al., 1987; Long et al., 2022; Blackford, 2023).

U-Pb zircon dating of undeformed and deformed rhyolitic dikes that intrude the NSRD footwall brackets the timing of ductile stretching and mylonitization between ~38 and 22 Ma (Lee et al., 2017). This timing range is supported by muscovite K-Ar, muscovite and K-feldspar 40 Ar/ 39 Ar, and zircon fission-track thermochronometry from the NSRD footwall, which defines eastward-younging cooling that is interpreted to reflect transport-parallel migration of extensional unroofing (Armstrong and Hansen, 1966; Lee et al., 1970; 1980; Lee and Sutter, 1991; Lee, 1995; Miller et al., 1999A; G'ebelin et al., 2011; 2015).

Despite a detailed understanding of the modern geometry of the Northern Snake Range, there is disagreement over the peak depths that Neoproterozoic-Cambrian rocks in the NSRD footwall were buried to, as well as the depths that they were residing at during the initiation of extension (cf. Miller et al., 1983; Bartley and Wernicke, 1984; Lewis et al., 1999; Cooper et al., 2010B; Wrobel et al., 2021; Hoiland et al., 2022). Earlier studies (Gans and Miller, 1983; Miller et al., 1983; Gans et al., 1985) interpreted that the NSRD originated at ~7 km depth, and that rocks in its footwall were never buried deeper than their regional stratigraphic depth range of ~7-12 km. This interpretation is supported by several field relationships described in Miller et al. (1999A) that indicate that rocks above and below the NSRD were stratigraphically contiguous prior to extension. Other studies (Lewis et al., 1999; Cooper et al., 2010B) have presented quantitative thermobarometry that suggest that NSRD footwall rocks in the eastern half of the range attained peak depths as great as ~20-30 km prior to extension, while others (Bartley and Wernicke, 1984; Wrobel et al., 2021) have presented

structural reconstructions that argue for more modest peak burial depths of $\sim 15-20$ km. Burial is attributed to Jurassic-Cretaceous thrusting and folding, although these studies present widely varying interpretations for the geometry and location of the structures that accomplished this burial.

This disagreement is further complicated by: 1) Paleo-geologic maps of the Paleozoic-Mesozoic sedimentary rocks exposed beneath a regional Eocene-Oligocene unconformity, which define minimal structural relief (\sim 2 km total) and erosion ($\leq \sim$ 1–3 km), and no evidence for large-throw thrust faults across this region (Armstrong, 1972; Gans and Miller, 1983; Long, 2012; 2015); 2) Cross section restorations across eastern Nevada and western Utah that did not find evidence for thrust faults or folds that could have accommodated more than ~3 km of structural burial (Long, 2019; Blackford et al., 2022); 3) Thermometry that defines upper-crustal, peak thermal field gradients as high as ~50 °C/km, which demonstrate that the ~500-650 °C peak temperatures attained by NSRD footwall rocks were attained at ~10-15 km depths in surrounding ranges (Miller and Gans, 1989; Blackford et al., 2022); and 4) Studies from the Northern Snake Range and Ruby-East Humboldt core complexes that postulate that pre-extensional depths of footwall rocks were much shallower than barometric estimates, allowing for the possibility that they experienced tectonic overpressure (Zuza et al., 2020; 2022; Hoiland et al., 2022).

4. Stratigraphy, structural geometry, and ductile thinning in the northern part of the Northern Snake Range

In the northern part of the range, the NSRD overlies Middle-Late Cambrian marble-dominated rock units that lie stratigraphically above the Early Cambrian Prospect Mountain Quartzite (Fig. 2) (Lee et al., 1999A, 1999B; Gans et al., 1999A). In the following sections, we describe the stratigraphy, metamorphic grade, structural geometry, and ductile thinning magnitude of these Middle-Late Cambrian rocks.

4.1. Stratigraphy of Middle-Late Cambrian rocks

Middle-Late Cambrian rocks in the NSRD footwall have been divided into five map units (Gans et al., 1999A, 1999B; Lee et al., 1999A, 1999B; 1999C; Wrobel et al., 2021): the Middle Cambrian Eldorado Limestone, Monte Neva Formation and Raiff Limestone, and the Late Cambrian Dunderberg Shale and Notch Peak Formation.

The Middle Cambrian Eldorado Limestone consists of light gray to white, bluff-forming calcite marble, which often exhibits alternating light gray and blue-gray laminations (Fig. 3A) and is locally massive (Lee et al., 1999A, 1999C). Stratigraphic thicknesses reported for the Eldorado Limestone range between 563 m (northern Egan Range) and 966 m (northern Duck Creek Range) (Young, 1960). The Middle Cambrian Monte Neva Formation is dominated by brown, slope-forming, calcareous schist, with interlayers of brown to tan, micaceous, calcite marble (Fig. 3B) (Lee et al., 1999A, 1999B; 1999C). Stratigraphic thicknesses reported for the Monte Neva Formation include 167 m in its type-section in the northern Egan Range (Young, 1960) and 180 m in the northwestern part of the Northern Snake Range (Lee et al., 1999C). The Middle Cambrian Raiff Limestone consists of light gray to blue-gray, bluff- to cliff-forming calcite marble with diagnostic alternating light gray and dark blue-gray laminations (Fig. 3C), which is interlayered with massive, gray-brown dolomite (Lee et al., 1999A, 1999C). Stratigraphic thicknesses reported for the Raiff Limestone include 850 m in the northern Egan Range (Young, 1960) and 720 m in the northern Schell Creek Range (Dechert, 1967). The Late Cambrian Dunderberg Shale is dominated by brown to tan, slope-forming, thinly laminated calcareous schist, which is interlayered with tan to medium gray, bluff-forming, micaceous, calcite marble (Fig. 3D) (Lee et al., 1999A, 1999B; 1999C). Stratigraphic thicknesses reported for the Dunderberg Shale range from 112 m (Northern Snake Range; measured in the NSRD hanging wall on cross section B-B' of Gans et al., 1999B), to 146-151 m

(northern Egan Range; Fritz, 1968; Young, 1960), to 183 m (central Schell Creek Range; Young, 1960). The Late Cambrian Notch Peak Formation consists of medium to dark gray, bluff-to cliff-forming calcite marble with diagnostic brown chert stringers and nodules (Fig. 3E). Stratigraphic thicknesses reported for the Notch Peak Formation in the Northern Snake Range vary between 468 m (measured in the NSRD hanging wall on cross section B-B' of Gans et al., 1999B) and 650–690 m (Gans and Miller, 1983; Lee et al., 1999C).

4.2. Metamorphism and magmatism in the NSRD footwall

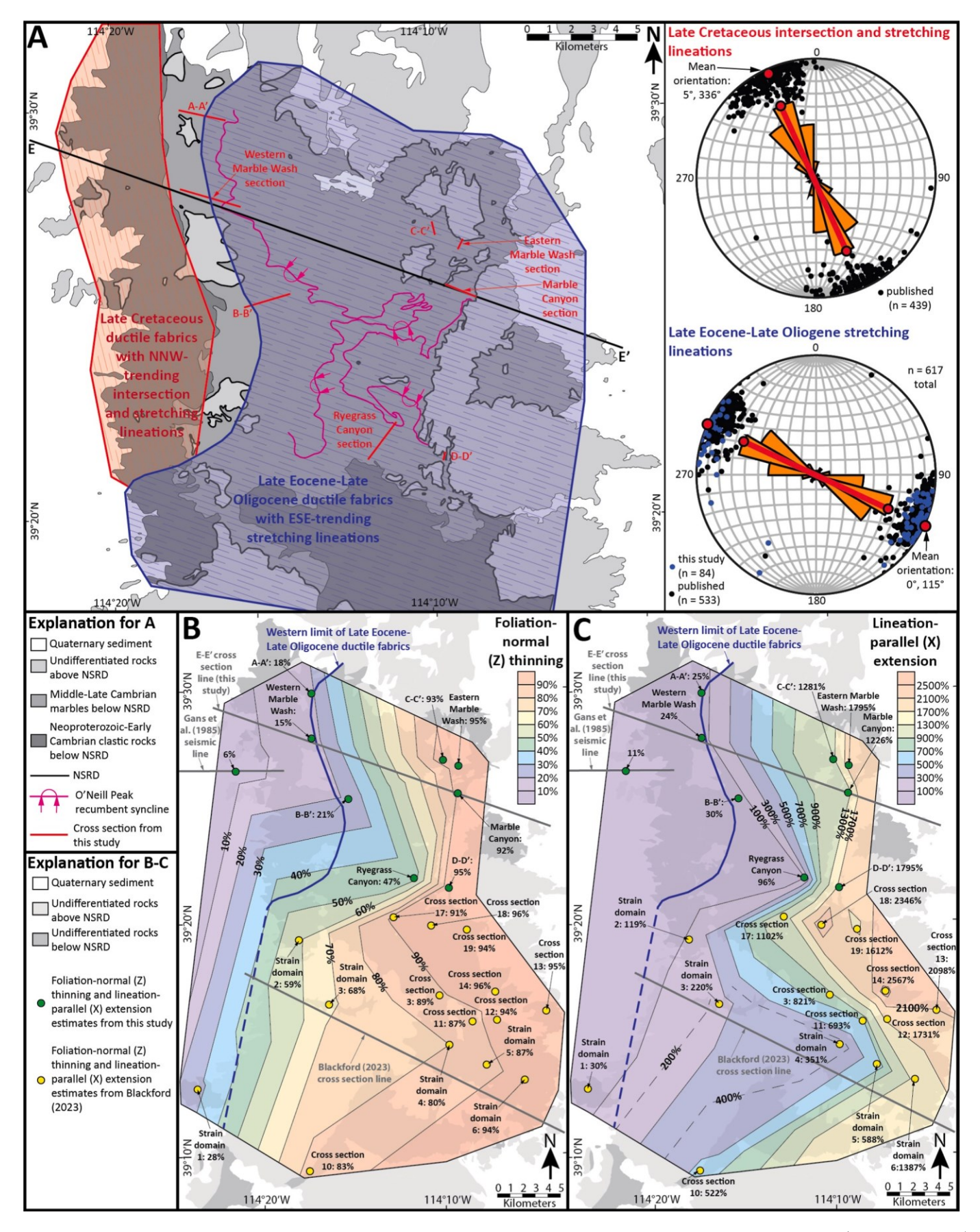
NSRD footwall rocks in the northern part of the range exhibit mineral assemblages that are indicative of upper greenschist-facies to lower amphibolite-facies peak metamorphism (Lee et al., 1999A, 1999B; Wrobel et al., 2021). In the western part of the range, metamorphic minerals in the Early Cambrian Prospect Mountain Quartzite and Pioche Shale include white mica, biotite, and locally garnet (Lee et al., 1999A; Wrobel et al., 2021). Metamorphic minerals in calcareous schist in the Middle Cambrian Monte Neva Formation and Late Cambrian Dunderberg Shale include white mica, phlogopite, biotite, clinozoisite, plagioclase, tourmaline, tremolite, and titanite (Lee et al., 1999A, 1999B; Gans et al., 1999A). Hoiland et al. (2022) collected peak metamorphic temperatures from Middle-Late Cambrian marble units in the NSRD footwall using Raman spectroscopy of carbonaceous material (RSCM) thermometry. They obtained peak temperatures between 475 \pm 51 $^{\circ}\text{C}$ and 569 ± 53 °C from the Eldorado Limestone, Monte Neva Formation, Raiff Limestone, and Notch Peak Formation in the eastern part of Marble Wash (six total samples), and they obtained 530 \pm 68 °C from an Ordovician Pogonip Group sample further to the west in Marble Wash (Fig. 2). The timing of peak metamorphism has not been dated in the northern part of the range, but amphibolite-facies peak metamorphism of Neoproterozoic-Early Cambrian rocks in the NSRD footwall in the southeastern part of the range is dated by U-Pb on monazite and zircon at ~78-84 Ma (Huggins and Wright, 1989; Cooper et al., 2010B) and Sm-Nd and Lu-Hf on garnet at ~88–91 Ma (Cooper et al., 2010B).

Neoproterozoic-Cambrian rocks in the NSRD footwall have been intruded by granite in multiple localities (Lee et al., 1999A, 1999B; 1999C; Gans et al., 1999B), with the highest density of exposed intrusions at the latitude of Smith Creek (Fig. 2). U-Pb zircon and monazite geochronology from granite intrusions in the northern part of the range defines a protracted magmatic history that spanned from ~101 to 75 Ma (Miller et al., 1988; Huggins, 1990; Lee et al., 1999C; Kenney, 2013; Womer and Thesis, 2017; Wrobel, 2020; Gottlieb et al., 2022). The overlap in the timing of peak metamorphism (~78–91 Ma) with granitic magmatism, as well as the spatial association of granite intrusions with high-grade metamorphism in adjacent ranges, suggests that Late Cretaceous magmatism was the primary heat source that led to peak metamorphic conditions in the Northern Snake Range (e.g., Miller and Bradfish, 1980; Barton et al., 1988; Miller and Gans, 1989; Barton, 1990; Blackford et al., 2022; Gottlieb et al., 2022).

The NSRD footwall also experienced Late Eocene magmatism, as indicated by rhyolitic dikes in the central and western parts of the range (Lee et al., 1999A, 1999B) (Fig. 2) that have been dated at \sim 37.5–37.8 Ma (U-Pb zircon; Lee et al., 2017). Mafic dikes also intrude NSRD footwall rocks (Fig. 2) (Lee et al., 1999A, 1999B), and one of these dikes from Marble Wash was dated at 40.4 \pm 1.4 Ma (U-Pb zircon; Cooper et al., 2010A).

4.3. Ductile fabrics in NSRD footwall rocks

On the northwestern flank of the range, the Prospect Mountain Quartzite locally exhibits tectonic foliations that dip steeper to the west relative to bedding, which produce NNW-trending intersection lineations with bedding (Lee et al., 1999A; Wrobel et al., 2021). These intersection lineations are subparallel to locally developed mineral stretching lineations observed on bedding planes (Lee et al., 1999A). We



(caption on next page)

Fig. 4. A) Simplified geologic map of the northern part of the Northern Snake Range, highlighting a western domain of ductile fabrics with NNW-trending intersection and stretching lineations generated by Late Cretaceous ductile shearing (highlighted in red) and an eastern domain of ductile fabrics with ESE-trending stretching lineations generated by Late Eocene-Late Oligocene ductile extension of the NSRD footwall (highlighted in blue). Equal area stereoplots and rose diagrams of lineation orientations (generated using Orient) in each domain are shown on the right and are compiled from Gans et al. (1999A; 1999B), Lee et al. (1999A; 1999B; 1999C), and this study. B) Simplified geologic map of the Northern Snake Range overlain by a contour map (contoured using linear interpolation) of the percent foliation-normal (Z strain axis) bulk ductile thinning measured in the NSRD footwall. Data from this study are shown in green, and data from the southern part of the range from Blackford (2023) are shown in yellow. Data from Blackford (2023) are from average measurements of their six strain domains and bulk thinning measurements of the Prospect Mountain Quartzite that we calculated from nine of their cross sections (cross sections 3, 10, 11, 12, 13, 14, 17, 18, 19). C) Simplified geologic map of the Northern Snake Range overlain by a contour map (contoured using linear interpolation) of the percent lineation-parallel (X strain axis) extension accommodated in the NSRD footwall; data from this study are shown in green, and data from the southern part of the range from Blackford (2023), which include average measurements from their six strain domains and measurements that we calculated from nine of their cross sections (3, 10, 11, 12, 13, 14, 17, 18, 19), are shown in yellow. X extension estimates from the cross sections in our study and the nine cross sections of Blackford (2023) were calculated using the measured Z thinning and assuming 3 ± 7% shortening in the Y direction, which is the average (±1σ) of 11 finite strain

plotted orientations of 439 of these intersection and stretching lineations (compiled from Lee et al., 1999A) on Fig. 4A, which define an average trend of 336°/156°. Miller et al. (1988) and Miller and Gans (1989) interpreted that these ductile fabrics were produced by low-strain, top-to-the-east, distributed layer-parallel shear above the basal d'ecollement of the Sevier fold-thrust belt, and Wrobel et al. (2021) interpreted that these ductile fabrics were approximately coeval with ~78–91 Ma peak metamorphism.

In the central and eastern parts of the range, Middle-Late Cambrian marbles are pervasively deformed by mylonitic, linear-planar ductile fabrics with strongly developed, ESE-trending mineral stretching lineations (Fig. 5A and B) (e.g., Lee et al., 1999B). We plotted orientations of 617 of these stretching lineations (compiled from: Lee et al., 1999A, 1999B; 1999C; Gans et al., 1999A, 1999B; this study) on Fig. 4A, which define an average trend of 115°/295°. This is similar to the 110- $125^{\circ}/290\text{--}305^{\circ}$ average trend of mineral stretching lineations in Neoproterozoic-Early Cambrian clastic rocks in the NSRD footwall in the southern part of the range (e.g., Miller et al., 1983; 1999B; Lee et al., 1987; Miller and Gans, 1999; Johnston, 2000), which are interpreted to define the average azimuth of Late Eocene-Late Oligocene ductile extensional deformation in the NSRD footwall (e.g., Miller et al., 1983; Lee et al., 1987). A set of ~37.5 Ma rhyolitic dikes in the northern part of the range are deformed by these ductile fabrics, whereas a ~22.5 Ma undeformed rhyolite dike in the southern part of the range post-dates fabric development, thereby bracketing the age range of extensional ductile shearing in the NSRD footwall (Lee et al., 2017).

4.4. Recumbent syncline and thrust fault system

Middle-Late Cambrian marbles in the NSRD footwall are deformed by a NNW-trending, eastward-opening, overturned syncline with a gently west-dipping axial plane (Lee, 1990; Lee et al., 1999A, 1999B), which Wrobel et al. (2021) named the O'Neill Peak recumbent syncline (Fig. 2). The NSRD cuts obliquely eastward across the syncline, and has removed much of the upper, overturned limb (Lee et al., 1999A; Wrobel et al., 2021). In the northwestern part of the range, rocks in the hinge zone of the syncline locally exhibit a gently west-dipping axial planar fabric (Lee et al., 1999A; Wrobel et al., 2021). To the east, the syncline is overprinted by Late Eocene-Late Oligocene ductile extensional fabrics, which transpose the fold to an isoclinal geometry with an axial plane that is sub-parallel to foliation (Lee, 1990; Lee et al., 1999A; Wrobel et al., 2021).

To the west of the O'Neill Peak recumbent syncline, several discontinuous traces of a gently west-dipping, top-to-the-east thrust fault system are mapped (Fig. 2) (Lee et al., 1999A; Wrobel et al., 2021). This fault system, which Wrobel et al. (2021) named the Eightmile thrust system, places the Early Cambrian Prospect Mountain Quartzite or Pioche Shale over the Middle Cambrian Eldorado Limestone. The Eightmile thrust system duplicates as much as ~200 m of stratigraphic section, exhibits low stratigraphic cutoff-angles, lacks matching hanging

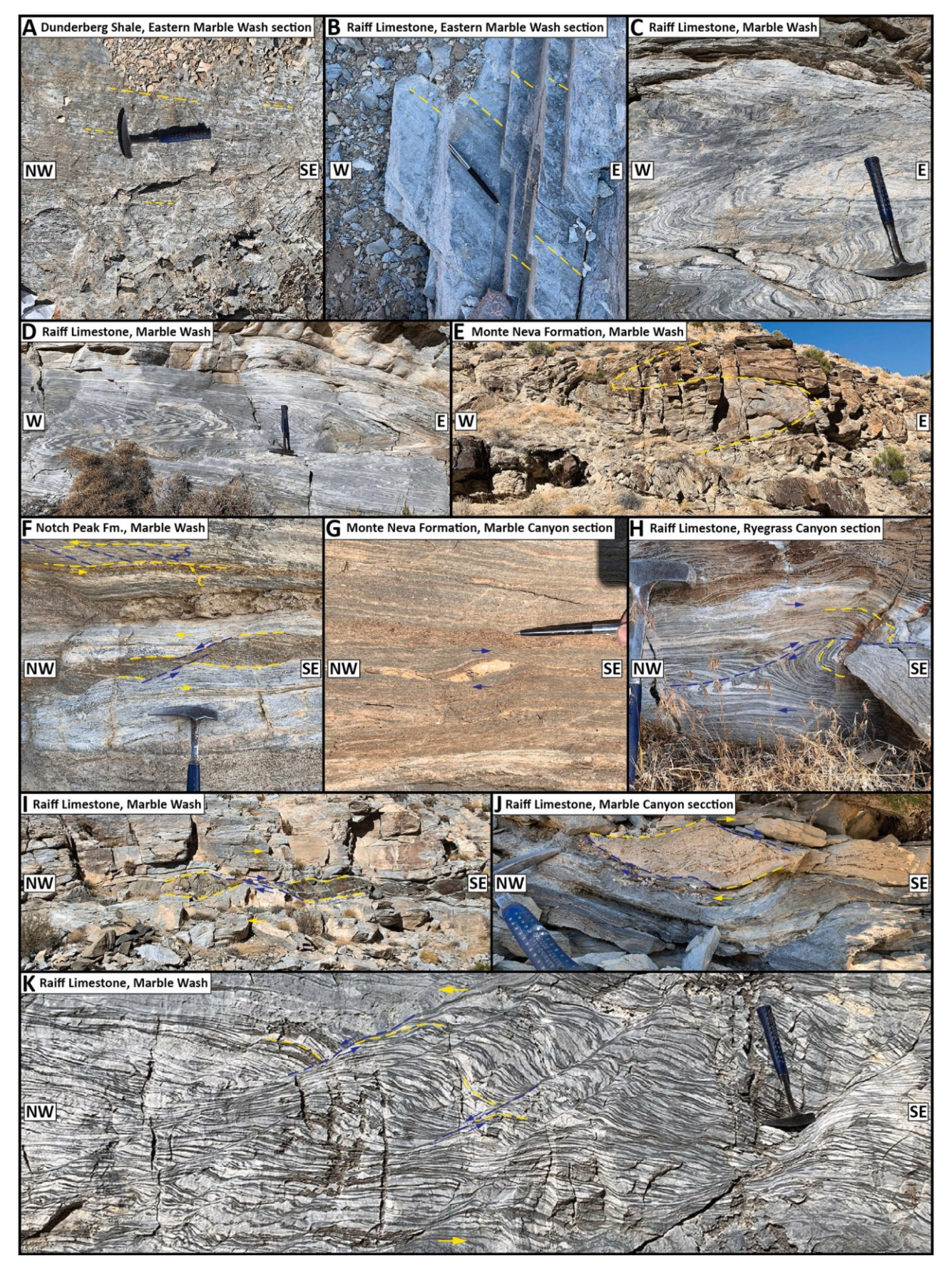
wall and footwall cutoffs, and has an inferred displacement magnitude of >1 km (Wrobel et al., 2021).

Wrobel et al. (2021) interpreted that the O'Neill Peak recumbent syncline was constructed during ~78–91 Ma peak metamorphism, based on syn-kinematic growth of phlogopite within axial planar fabrics in its hinge zone, and they interpreted that displacement on the Eightmile thrust system was genetically related to construction of the syncline.

4.5. Ductile thinning magnitudes measured from cross sections

To measure the deformed thicknesses of Middle-Late Cambrian rock units in the NSRD footwall across the northern part of the range, we mapped and drafted cross sections along the Western Marble Wash section (Fig. 6), Ryegrass Canyon section (Fig. 7), Eastern Marble Wash section (Figs. 8 and 9A), and Marble Canyon section (Fig. 9B and 10) (geologic map locations shown on Fig. 2). We also used published mapping (Lee et al., 1999A, 1999B; 1999C) to draft four additional cross sections (A-A', B-B', C-C', D-D'; Fig. 11) (lines of section shown on Fig. 2). Using the published stratigraphic thicknesses listed above (section 4.1), the Monte Neva Formation (174 \pm 7 m), Raiff Limestone (785 \pm 65 m) and Dunderberg Shale (148 \pm 36 m) yield a combined thickness of 1107 ± 107 m (Table 1; Fig. 12A). We measured the deformed thicknesses of these three units on each of our eight cross sections and compared them to their stratigraphic thickness range to calculate percent thinning. For our calculations, we assumed that the ranges of published stratigraphic thicknesses that we compiled for these three units are representative of their regional stratigraphic thickness variation in east-central Nevada. Thinning of individual units varies on each cross section, so we found it more effective to use the 'bulk thinning' of all three units as the most representative unit of measure. The Western Marble Wash section yielded a 935 m cumulative thickness, corresponding to 15 \pm 8% bulk thinning (Fig. 12B). This is similar to the 900 m thickness (18 \pm 8% bulk thinning) obtained on cross section A-A' ~4 km along-strike to the north and the 869 m thickness (21 \pm 8% bulk thinning) obtained on cross section B-B' ~5 km along-strike to the southeast (Table 1; Figs. 2 and 11). To the east, thinning increases significantly. The Ryegrass Canyon section yielded a cumulative thickness of 585 m (47 \pm 5% bulk thinning) (Fig. 12C), and the four easternmost cross sections yielded thicknesses between 54 and 88 m, corresponding to 92-95% bulk thinning (C-C': 81 m, 93 ± 1% bulk thinning; Eastern Marble Wash section: 60 m, $95 \pm 1\%$ bulk thinning; Marble Canyon section: 88 m, $92 \pm 1\%$ bulk thinning; D-D': 54 m, 95 \pm 1% bulk thinning) (Table 1; Figs. 11 and

The dramatic eastward increase in ductile thinning in the NSRD footwall (contoured on Fig. 4B) is consistent with the spatial distribution of Late Eocene-Late Oligocene extensional ductile fabrics (Fig. 4A). Cross sections A-A', B-B', and the Western Marble Wash section (~15–21% thinning) overlap the western limit of Late Eocene-Late Oligocene extensional ductile fabrics (Lee et al., 2017). The remaining sections lie entirely within the domain of Late Eocene-Late Oligocene



(caption on next page)

Fig. 5. Photographs of mineral stretching lineations (A-B), isoclinal folds (C-E), and shear-sense indicators (F-K) observed in Middle-Late Cambrian rocks in the Northern Snake Range. A) Mineral stretching lineations defined by shape-preferred elongation of mica porphyroblasts on a micaceous parting within a marble interlayer in the Dunderberg Shale (view is looking down on a foliation plane; 39.44444 °N, 114.14992 °W). B) Mineral stretching lineations defined by shape-preferred elongation of recrystallized calcite within marble of the Raiff Limestone (view is looking down on a foliation plane; 39.44425 °N, 114.15056 °W). C) Folded compositional laminations within marble of the Raiff Limestone, including several isoclinal folds in the center part of the photograph (39.44389 °N, 114.14308 °W). D) Isoclinally folded compositional laminations within marble of the Raiff Limestone (39.44389 °N, 114.14308 °W). E) Isoclinally folded marble boudin within the Monte Neva Formation (39.44831 °N, 114.16169 °W). F) Top-to-NW SC fabric (top left part of photograph) and asymmetrically sheared boudins (center part of photograph) that are deformed by a top-down-to-NW C'-type extensional shear band, consistent with an overall top-to-NW shear-sense (Notch Peak Formation marble; 39.44223 °N, 114.11308 °W). G) Calcite vein within marble of the Monte Neva Formation that is sheared into a top-to-SE asymmetric fold that is deformed by a top-to-SE, thrust-sense shear zone (marble of the Raiff Limestone; 39.43700 °N, 114.13400 °W). I) Asymmetrically sheared boudins of a mafic dike within a marble of the Raiff Limestone that are deformed by a top-down-to-SE C'-type extensional shear band, consistent with an overall top-to-SE shear-sense (39.44431 °N, 114.13010 °W); K) Top-down-to-SE C'-type extensional shear bands, consistent with an overall top-to-NW shear-sense (39.44431 °N, 114.15031 °W); K) Top-down-to-NW C'-type extensional shear bands in marble of the Raiff Limestone, which are consistent with an overall top-to-NW shear-sense (39.4

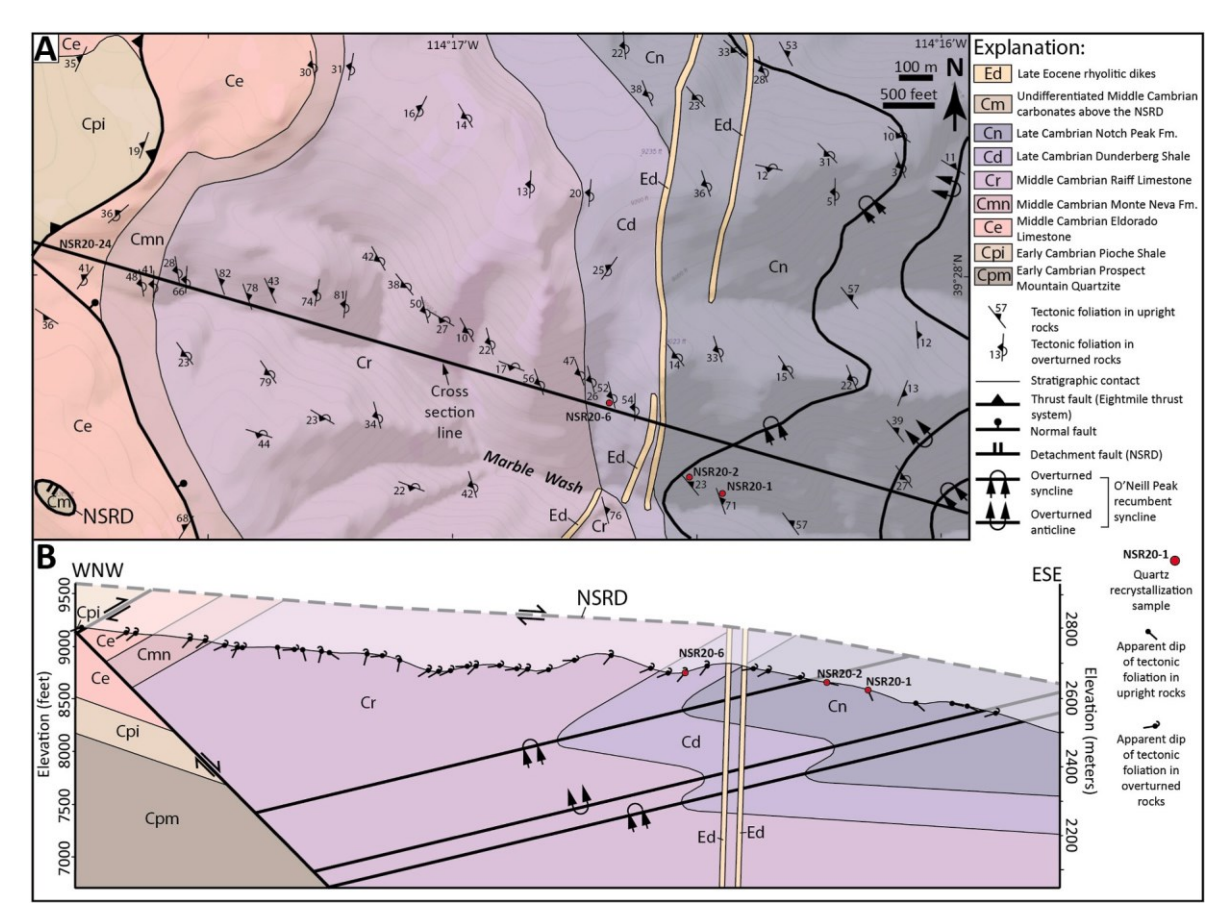


Fig. 6. A) Detailed geologic map and B) cross section of the Western Marble Wash section. Mapping is compiled from Lee et al. (1999A) and our measurements proximal to the cross section line. Here, the O'Neill Peak recumbent syncline exhibits two underlying parasitic fold axes, resulting in a syncline-anticline-syncline geometry (Lee et al., 1999A; Wrobel et al., 2021).

fabrics, with ductile thinning increasing eastward from \sim 47% to \sim 92 \rightarrow 95%.

4.6. Boudinage and shear-sense indicators

Middle-Late Cambrian marbles in the eastern part of the range exhibit boudinage and shear-sense indicators that document the kinematics and provide insight into the deformation mechanisms of Late Eocene-Late Oligocene ductile shearing. The Monte Neva Formation and Dunderberg Shale, which are calcareous schist-dominated units situated between marble-dominated units above and below, have been deformed into megaboudins in Marble Wash and Marble Canyon (Figs. 13 and 14) (Lee et al., 1999B; Gans et al., 1999A). There are 24 megaboudins

mapped in these drainages, which have lineation-parallel lengths typically between 140 and 470 m (average 290 m), lineation-normal lengths typically between 100 and 360 m (average 200 m), and foliation-normal thicknesses typically between 15 and 25 m. On the northern side of Marble Wash, megaboudins of the Dunderberg Shale are separated by lineation-parallel distances as great as ~1 km, resulting in direct structural contact between the Raiff Limestone and Notch Peak Formation along much of the northern side of the wash (Figs. 13 and 14A) (Lee et al., 1999B).

Outcrop-scale boudins are also common within the Middle-Late Cambrian section, including boudins of marble within the Monte Neva and Notch Peak Formations (Fig. 5E and F) and boudins of dolomite layers and mafic dikes within the Raiff Limestone (Fig. 5I and J, 9A).

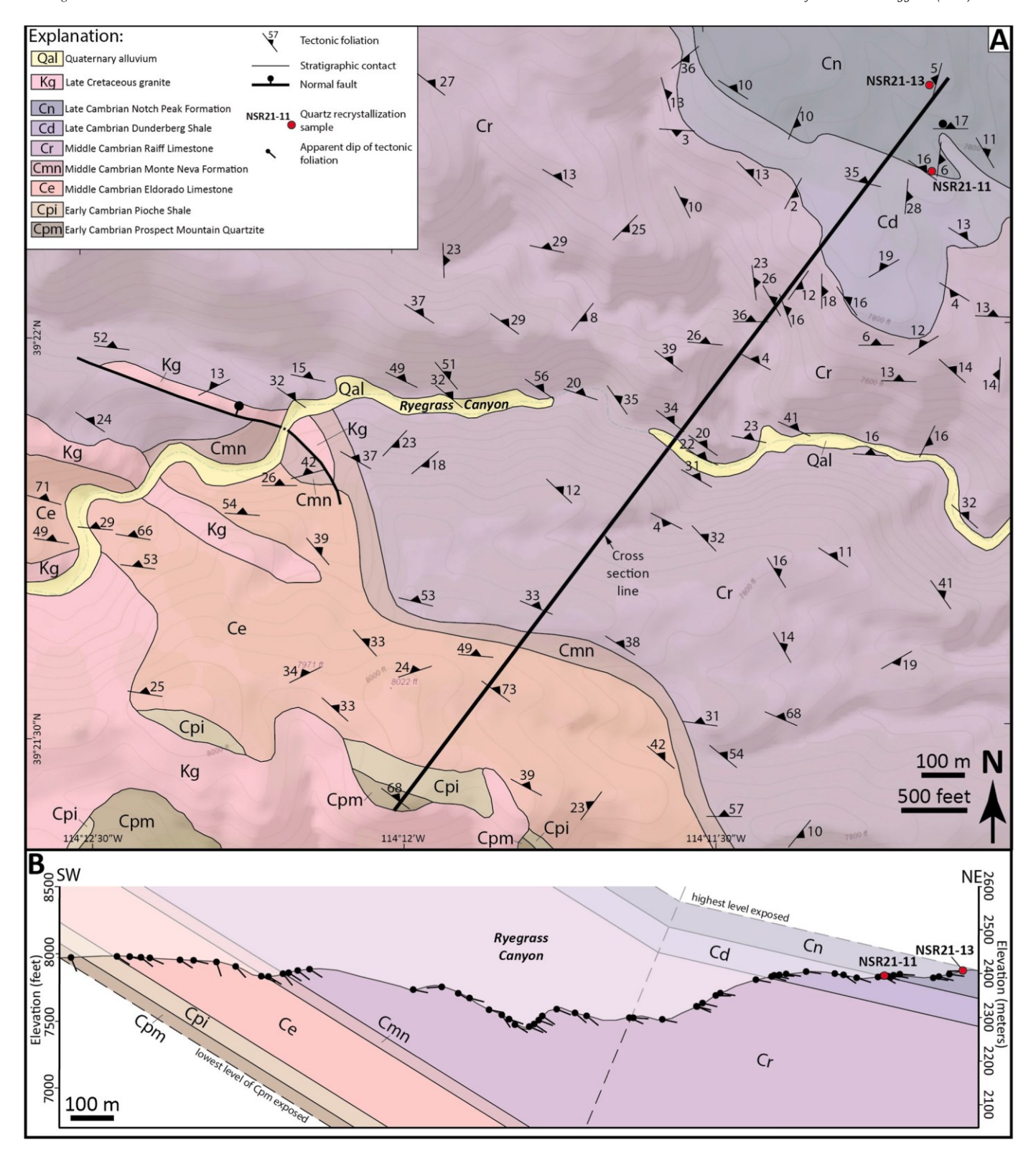


Fig. 7. A) Detailed geologic map and B) cross section of the Ryegrass Canyon section. Mapping is compiled from Lee et al. (1999C) and our measurements proximal to the cross section line.

Outcrop-scale isoclinal folds are locally observed within boudins (Fig. 5E) or defined by compositional laminations in marbles of the Eldorado Limestone and Raiff Limestone (Fig. 5C and D).

Outcrop-scale shear-sense indicators are prevalent in Middle-Late Cambrian rocks in the eastern parts of Marble Wash and Marble Canyon, and include asymmetrically sheared boudins, SC fabrics, sigma objects, asymmetric folds, and C'-type extensional shear bands (Fig. 5F-K). Within individual outcrops, both top-to-ESE and top-to-WNW shear-sense indicators are present (e.g., Cooper et al., 2010A), but top-to-ESE indicators are by far the most numerous, accounting for 33 of the 39 (85%) shear-sense indicators that we observed.

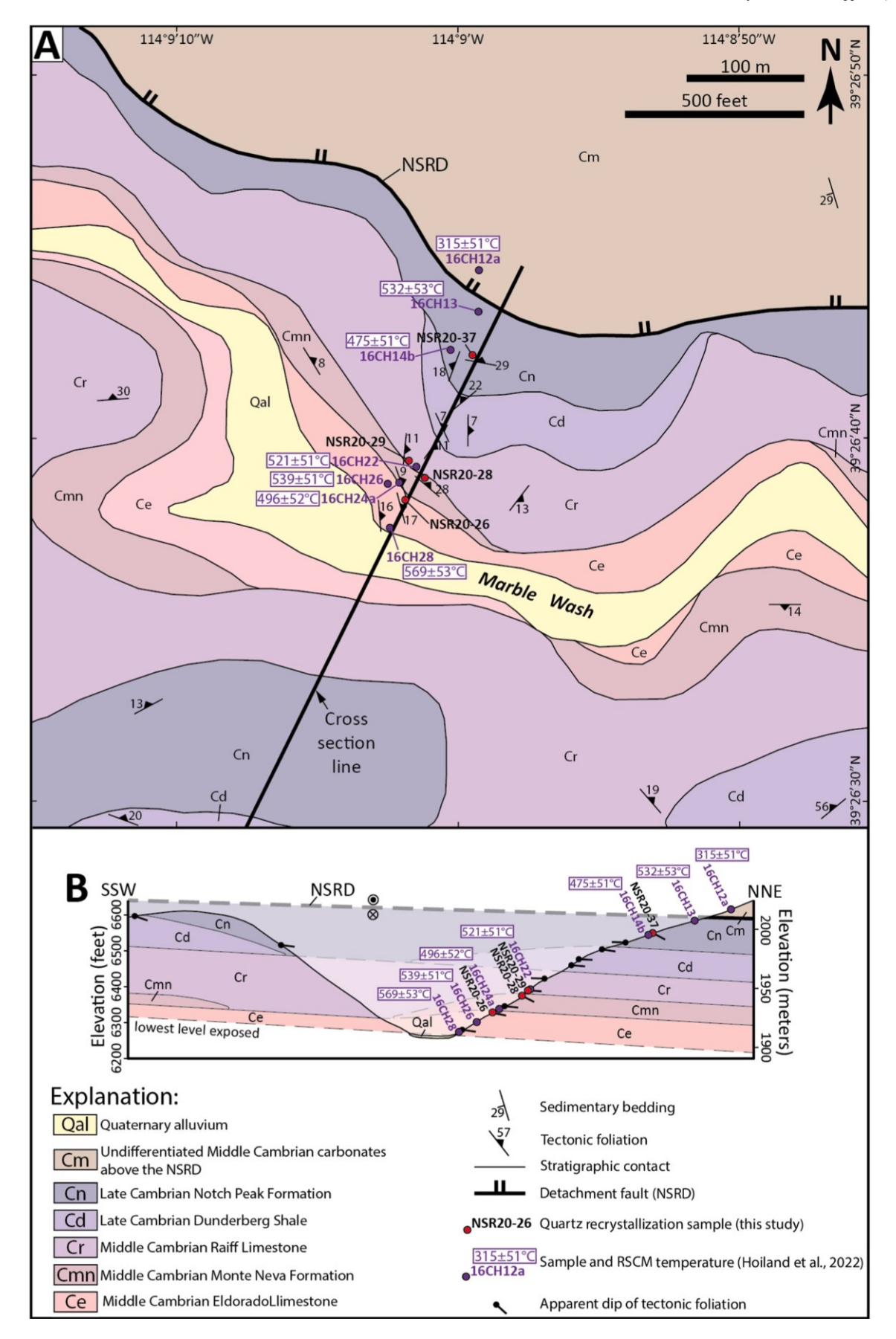


Fig. 8. A) Detailed geologic map and B) cross section of the Eastern Marble Wash section. Mapping is compiled from Lee et al. (1999B) and our measurements proximal to the cross section line. Sample locations and RSCM peak temperatures from Hoiland et al. (2022) are shown.

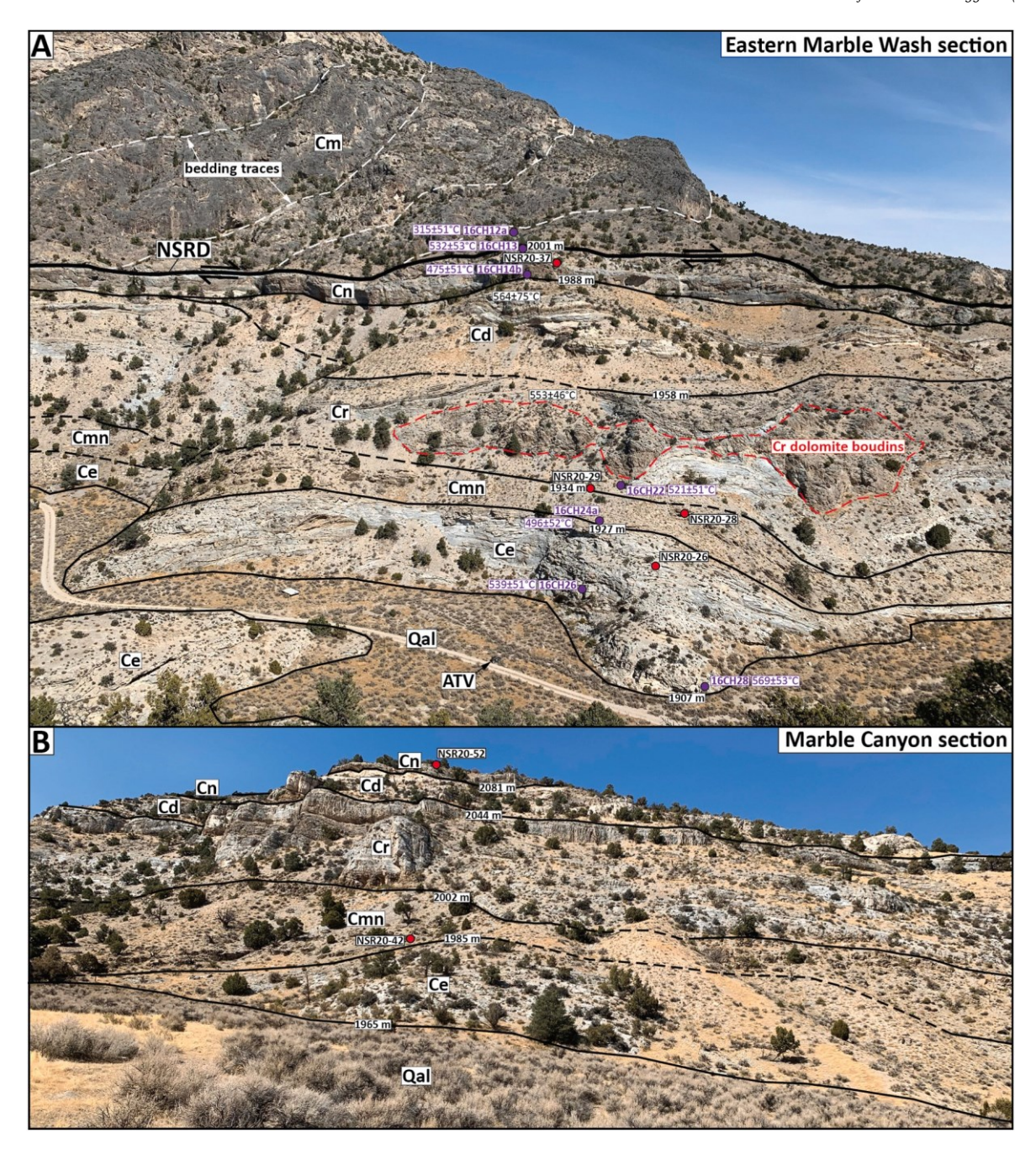


Fig. 9. Annotated photographs of the A) Eastern Marble Wash section (facing NNE) and B) Marble Canyon section (facing WNW), showing geologic contacts, quartz recrystallization sample locations from this study (red dots), and RSCM sample locations (purple dots) and peak temperatures from Hoiland et al. (2022). See Fig. 8 for a guide to rock units. Abbreviations on A: NSRD = Northern Snake Range d`ecollement, ATV = all-terrain vehicle. (For interpretation of the references to colour in this figure legend, the reader is referred to the Web version of this article.)

5. Deformation geometry from a range-wide cross section

To illustrate the deformation geometry across the width of the northern part of the Northern Snake Range, we drafted cross section E-E' (Fig. 15A; line of section shown on Fig. 2), which is supported by the 1:24,000-scale mapping of Lee et al. (1999A; 1999B) and Gans et al. (1999A), as well as our mapping in the Western Marble Wash and Marble Canyon sections (Figs. 6 and 10). The line of section for E-E' is oriented parallel to the 295°/115° average azimuth of Late Eocene-Late Oligocene mineral stretching lineations (Fig. 4A). Cross section E-E' was drafted from the western extent to the eastern extent of exposed bedrock in the northern part of the Northern Snake Range (Fig. 2) and has a total length of 28.7 km.

The geometry of the NSRD is constrained by eight klippen of hanging wall rocks that intersect or lie within ≤0.5 km of the section line (Fig. 2). These klippen define a 15°W average dip for the NSRD in the western part of the range and a 4°E average dip across the central and eastern parts (Fig. 15A). NSRD hanging wall rocks along and proximal to the section line are dominated by unmetamorphosed Middle Cambrian carbonates, which are stratigraphically equivalent to the combined Eldorado Limestone-Monte Neva Formation-Raiff Limestone section (Lee et al., 1999A, 1999B; Gans et al., 1999A). These unmetamorphosed carbonates structurally overlie their metamorphosed stratigraphic equivalents in the footwall across a 17.5 km NSRD-parallel distance, which provides a minimum displacement magnitude for the NSRD.

In the NSRD footwall in the western part of the range, the Early

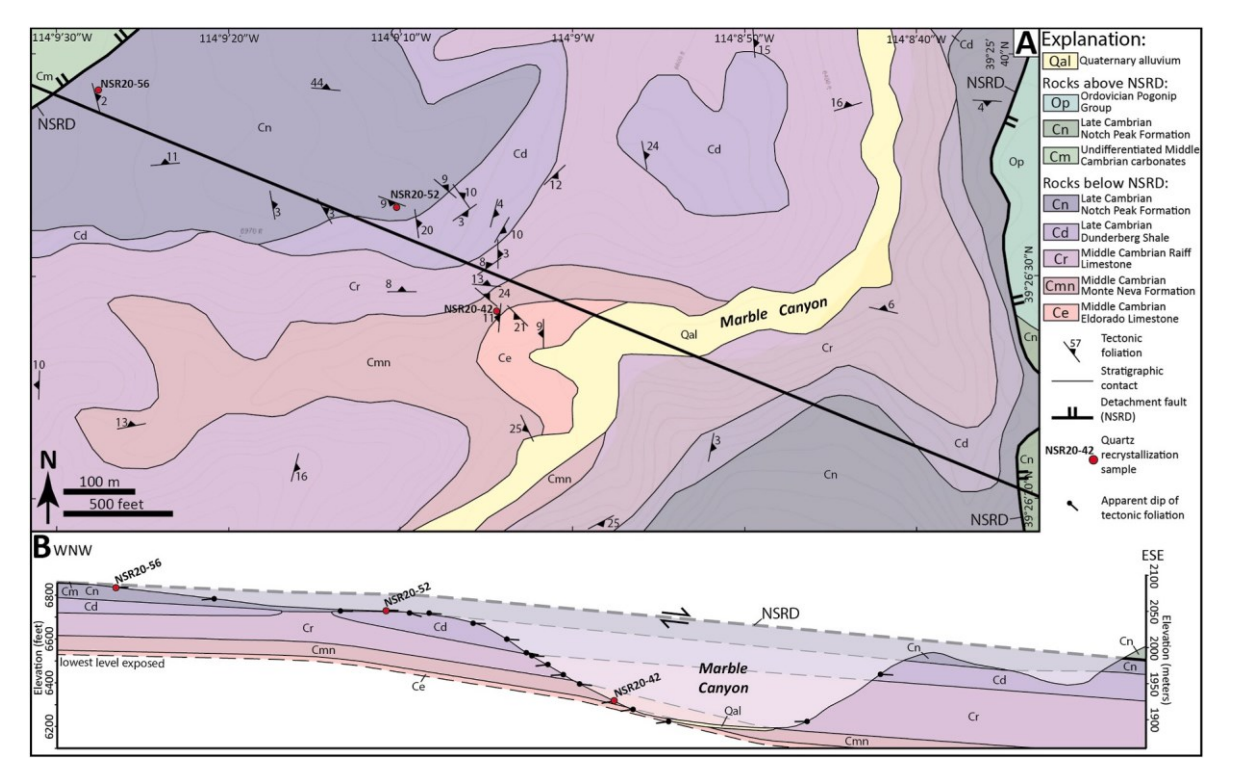


Fig. 10. A) Detailed geologic map and B) cross section of the Marble Canyon section. Mapping is compiled from Lee et al. (1999B) and our measurements proximal to the cross section line.

Cambrian Prospect Mountain Quartzite is folded into an open anticline (Fig. 15A). The NSRD overlies the Early Cambrian Pioche Shale at the western edge of the range and cuts down-section toward the ESE through the Prospect Mountain Quartzite until it crosses the anticline axis. To the east of the anticline axis, the NSRD cuts upsection through the Prospect Mountain Quartzite, Pioche Shale, and Eldorado Limestone until it intersects an east-dipping normal fault that accommodated ~1.5 km of displacement prior to motion on the NSRD (Lee et al., 1999A). In the hanging wall of this normal fault, overturned Middle-Late Cambrian marble units are exposed in the upper limb of the O'Neill Peak recumbent syncline. The western limit of Late Eocene-Late Oligocene extensional ductile fabrics is located 1.4 km to the east of the trace of the normal fault (Fig. 15A) (Lee et al., 2017). Parasitic overturned anticline and syncline axes are exposed structurally beneath the O'Neill Peak recumbent syncline axis. Eastward of the lower overturned syncline axis, the NSRD exhibits an approximate footwall flat within the Late Cambrian Notch Peak Formation until the eastern edge of the cross section.

6. Model for finite strain in the NSRD footwall

The NSRD footwall exhibits an impressive strain gradient across the range, which is expressed by eastward-increasing structural thinning of Cambrian metasedimentary rocks (Fig. 15A). On the western flank of the range, distributed linear-planar fabrics with NNW-trending intersection and stretching lineations (Fig. 4A) have been attributed to low-strain, east-vergent, Late Cretaceous ductile shearing (Miller et al., 1988; Miller and Gans, 1989; Lee, 1990). On the interpreted seismic reflection cross section of Gans et al. (1985), which projects 3–5 km to the south of the E-E' section line (Fig. 2), we measured a 1150 m thickness for the Prospect Mountain Quartzite beneath the western flank of the range. This corresponds to 6 \pm 2% bulk thinning from the 1220 \pm 30 m average regional stratigraphic thickness for this rock unit (calculated from the average (\pm 1 σ) of thicknesses reported in the Schell Creek, Deep Creek, and Southern Snake Ranges by Young, 1960, Whitebread, 1969,

Rodgers, 1987, Miller et al., 1994, Blackford et al., 2022, and Long et al., 2022). We interpret that this thinning was accomplished during Late Cretaceous shearing, as this part of the range was not overprinted by Late Eocene-Late Oligocene extensional ductile fabrics (Fig. 4A). In the Western Marble Wash section, we measured $15 \pm 8\%$ bulk thinning of the combined Monte Neva Formation, Raiff Limestone, and Dunderberg Shale (thinned to 935 m total) in the overturned limb of the O'Neill Peak recumbent syncline. We interpret that this thinning was accommodated during the Late Cretaceous construction of the syncline and was achieved in part by local development of axial-planar cleavage (Lee et al., 1999A; Wrobel et al., 2021).

Linear-planar fabrics with ESE-trending stretching lineations, which characterize Late Eocene-Late Oligocene extensional ductile shearing of the NSRD footwall (e.g., Miller et al., 1983), first appear 0.5 km to the west of the O'Neill Peak recumbent syncline axis (Fig. 15A) and are ubiquitous from this point eastward (Fig. 4A). In the eastern part of the range, we measured 92 \pm 1% bulk thinning of the combined Monte Neva Formation, Raiff Limestone, and Dunderberg Shale (thinned to 88 m total) in the Marble Canyon section.

To measure the magnitude of ductile strain in the NSRD footwall, we divided cross section E-E', which is oriented parallel to the 115°/295° average azimuth of Late Eocene-Late Oligocene mineral stretching lineations, into a simplified five-domain strain model (Fig. 15B and C). Strain domains were defined based on changes in measured strain magnitude. Strain domain 1 spans from the western edge of the cross section to a point that bisects the distance to the western edge of the Western Marble Wash section (Figs. 2 and 15A), and has an NSRDparallel length of 3.9 km. We assumed that the $6 \pm 2\%$ bulk thinning of the Prospect Mountain Quartzite at the western edge of the cross section (measured from Gans et al., 1985) is consistent across the full width and height of strain domain 1. Strain domain 2 extends from the eastern edge of strain domain 1 to the eastern contact of the Dunderberg shale in the Western Marble Wash section (Figs. 2 and 15A). Strain domain 2 has an NSRD-parallel length of 5.7 km. For this strain domain, we assumed that the $15 \pm 8\%$ bulk thinning that we calculated in the

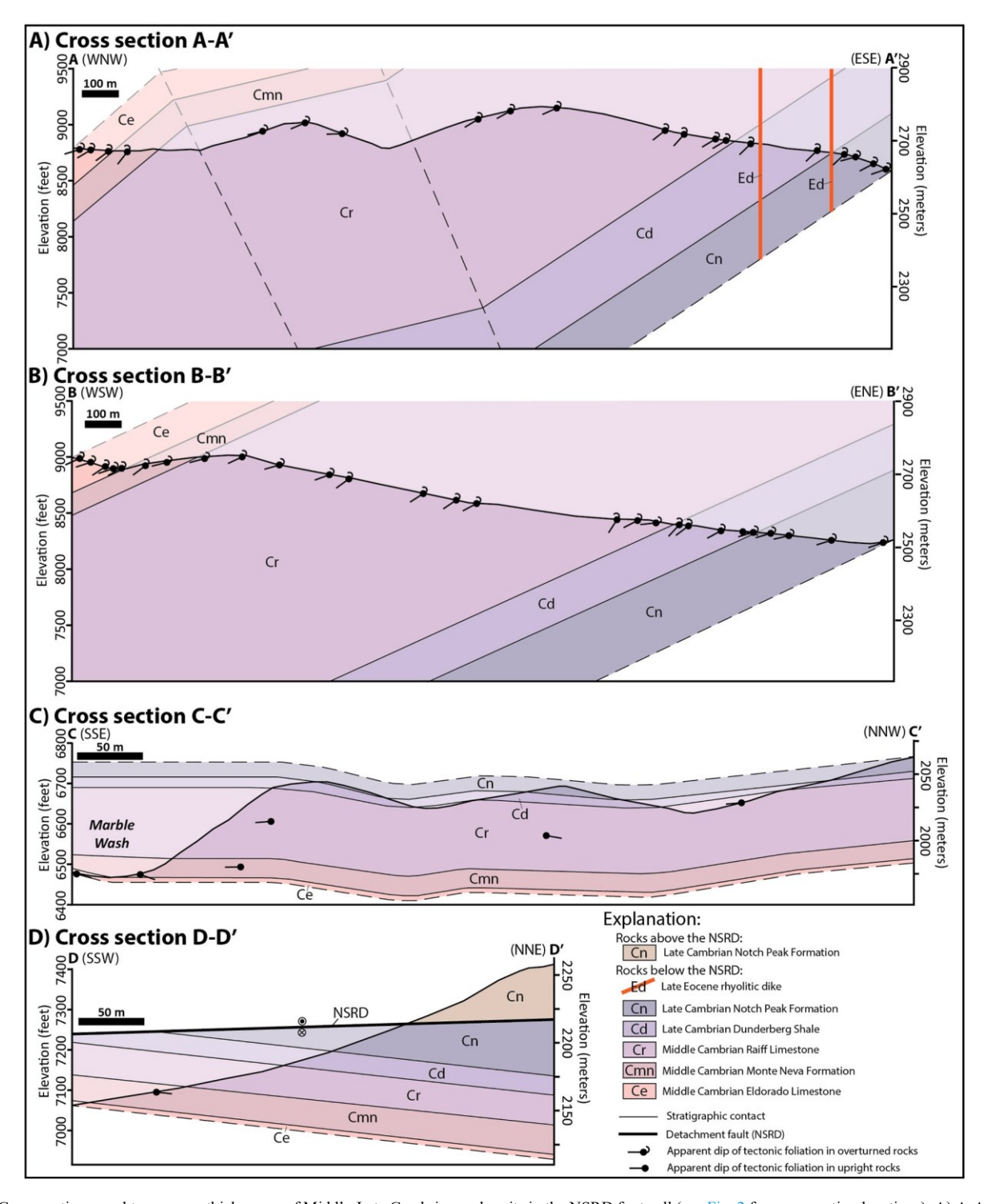


Fig. 11. Cross sections used to measure thicknesses of Middle-Late Cambrian rock units in the NSRD footwall (see Fig. 2 for cross section locations). A) A-A', which is supported by the mapping of Lee et al. (1999A), is located ~3.5 km to the north of the Western Marble Wash section; B) B-B', which is supported by the mapping of Lee et al. (1999B), is located ~8.5 km to the west of the Marble Canyon section; C) C-C', which is supported by the mapping of Lee et al. (1999B), is located ~1.5 km to the west of the Eastern Marble Wash section, and D) D-D', which is supported by the mapping of Lee et al. (1999C), is located ~3.0 km to the east of Ryegrass Canyon section. Dashed contacts represent the structurally lowest and highest levels exposed on the area of each cross section.

overturned limb of the O'Neill Peak recumbent syncline in the Western Marble Wash section is representative for the lower, upright limb and is consistent across the full width and height of strain domain 2.

Rocks within strain domains 1 and 2 were not overprinted by Late Eocene-Late Oligocene ductile fabrics, and therefore we interpret that the low-magnitude bulk thinning that they experienced was entirely accomplished during Late Cretaceous ductile deformation (e.g., Miller

et al., 1988; Wrobel et al., 2021). The maximum extension direction (i. e., X strain axis) during Late Cretaceous deformation is constrained by the 336°/156° mean trend of intersection and stretching lineations in the western part of the range (Fig. 4A). However, we cannot calculate 3D finite strain ellipsoids for these two domains because of the absence of data that constrain the magnitude of extension or shortening in the lineation-normal direction (i.e., Y strain axis).

Rock unit	Undeformed	Western Marble Wash section	arble Wash	Ryegrass Canyon section	nyon	Marble Canyon section	yon section	Eastern Marble Wash section	ble Wash	Cross section A-	n A-	Cross section B-B'	n B-B'	Cross section C-C'	n C-C'	Cross section D-D'	n D-D'
	stratigraphic	Deformed		Deformed		Deformed		Deformed		Deformed		Deformed		Deformed		Deformed	
	thickness (m)	thickness (m)	Thinning (%)	thickness (m)	Thinning (%)	thickness (m)	Thinning (%)	thickness (m)	Thinning (%)	thickness (m)	Thinning (%)	thickness (m)	Thinning (%)	thickness (m)	Thinning (%)	thickness (m)	Thinning (%)
Notch Peak	579 ± 111	115		09		25		29		134		91		2		24	
Formation (Cn)		minimum		minimum		minimum		minimum		minimum		minimum		minimum		minimum	
Dunderberg	148 ± 36	110	21 ± 19	09	57 ± 10	42	70 ± 7	24	83 ± 4	165	-19 ± 29	110	21 ± 19	10	93 ± 2	15	89 ± 3
Raiff Limestone	785 ± 65	720	∞ +I ∞	495	37 ± 5	26	97 ± 0.3	20	97 ± 0.2	659	15 ± 7	701	10 ± 7	55	93 ± 0.6	24	97 ± 0.3
(Cr) Monte Neva	174 ± 7	105	39 ± 2	30	83 ± 1	20	88 ± 0.4	16	91 ± 0.2	76	56 ± 2	58	67 ± 1	16	91 ± 0.3	15	91 ± 0.3
Formation (Cmn)																	
Eldorado	765 ± 202	120		145	80 ± 5	7		23		73		85		3		2	
Limestone (Ce)		minimum				minimum		minimum		minimum		minimum		minimum		minimum	
Total: Cmn + Cr	1107 ± 107	935	15 ± 8	585	47 ± 5	88	92 ± 1	09	95 ± 1	006	18 ± 8	698	21 ± 8	81	93 ± 1	54	95 ± 1
ح +																	

Rocks within strain domains 3-5 have been pervasively overprinted by Late Eocene-Late Oligocene ductile fabrics, and the 295°/115° mean trend of stretching lineations in these rocks (Fig. 4A) constrains the maximum extension direction (i.e., the X strain axis of Late Eocene-Late Oligocene ductile extensional shearing). Strain domains 3 and 4 were defined by linearly interpolating the bulk thinning magnitude between strain domain 2 (15 \pm 8%) and the Marble Canyon section (92 \pm 1%) and bisecting the 11.2 km NSRD-parallel distance between these localities. Strain domains 3 and 4 each have NSRD-parallel lengths of 5.6 km and have interpolated bulk thinning magnitudes of 41 \pm 5% and 66 \pm 2%, respectively (Figs. 2 and 15B). Strain domain 5 spans from the upper contact of the Dunderberg Shale in the Marble Canyon section to the eastern edge of the cross section, and has an NSRD-parallel length of 8.2 km. We assumed that the $92 \pm 1\%$ bulk thinning that we measured in the Marble Canyon section is representative across the full width of strain domain 5.

To estimate finite strain ellipsoids for strain domains 3-5, we assumed that the rocks in these strain domains experienced a similar magnitude of Late Eocene-Late Oligocene, lineation-normal (Y strain axis) shortening as measured in Neoproterozoic-Lower Cambrian clastic rocks in the NSRD footwall in the southern part of the range, which is 3 ± 7% (i.e., slightly constrictional to plane-strain deformation). This represents the average $(\pm 1\sigma)$ Y shortening for the 11 finite strain ellipsoids measured in the southern part of the range by Lee et al. (1987, their Table 1), which we calculated by comparing the relative lengths of each finite strain ellipsoid to the diameter of a sphere with the same volume (i.e., assuming constant-volume deformation; Ramsay, 1967; Ramsay and Huber, 1983) (also see Table 2). We combined the foliation-normal bulk thinning magnitudes measured in strain domains 3-5 (Z strain axis) with the 3 \pm 7% average lineation-normal (Y strain axis) shortening to estimate the corresponding percent lineation-parallel (X strain axis) extension and tectonic strain ratios (Rs_{XZ} and Rs_{YZ}) of the finite strain ellipsoids for each strain domain by restoring each ellipsoid to a sphere with the same volume (i.e., assuming constant-volume deformation; Ramsay, 1967; Ramsay and Huber, 1983). Strain domains 3, 4, and 5 yielded finite strain ellipsoids with Rsxz values of 3.1 \pm 0.7, 9.1 \pm 1.7, and 172 \pm 53 and X extension values of 78 \pm 28%, 207 \pm 40%, and 1226 \pm 256%, respectively (Fig. 15B) (error values for X extension and Rs_[XZ] were calculated using the error ranges of % Z shortening and % Y shortening for each strain domain; see Table 2). These ellipsoids represent an estimate of the cumulative strain accomplished by both Late Cretaceous and Late Eocene-Late Oligocene ductile deformation.

To estimate the magnitude of ductile extension of the NSRD footwall that was accomplished only during Late Eocene-Late Oligocene ductile extension, we restored strain domains 3-5 to an approximate Late Cretaceous geometry (Fig. 15C; Table 2). To perform this restoration, we assumed that the low-magnitude Late Cretaceous bulk thinning recorded in the western portion of the range also likely affected the rocks in strain domains 3-5 prior to their overprinting by Late Eocene-Late Oligocene ductile extension, as previously interpreted for the NSRD footwall in the southern part of the range (e.g., Miller et al., 1988; Miller and Gans, 1989). We restored strain domains 3-5 to a geometry that matches the 15 \pm 8% bulk foliation-normal thinning (Z strain axis) measured in strain domain 2 (Fig. 15C). Using the $3 \pm 7\%$ average Y shortening measured from the NSRD footwall in the southern part of the range (Lee et al., 1987), this corresponds to restoration of strain domains 3–5 to a finite strain ellipsoid with an Rs_[XZ] of 1.5 \pm 0.4, 24 \pm 21% X extension, and 15 \pm 8% Z shortening. Restoration of strain domains 3, 4, and 5 to this ellipsoid yielded pre-Late Eocene, NSRD-parallel lengths of 4.1 ± 1.3 km, 2.3 ± 0.7 km, and 0.8 ± 0.3 km, respectively. Combining these lengths yielded a total restored NSRD-parallel length of 7.3 \pm 2.2 km (Fig. 15C). Comparing the modern lengths of 5.6 km, 5.6 km, and 8.2 km of strain domains 3-5 to their restored lengths (Fig. 15B and C) yielded 1.5 \pm 1.3 km (52 \pm 47%), 3.3 \pm 0.7 km (160 \pm 75%), and 7.4 \pm $0.3 \text{ km} (1035 \pm 394\%)$ of Late Eocene-Late Oligocene extension,

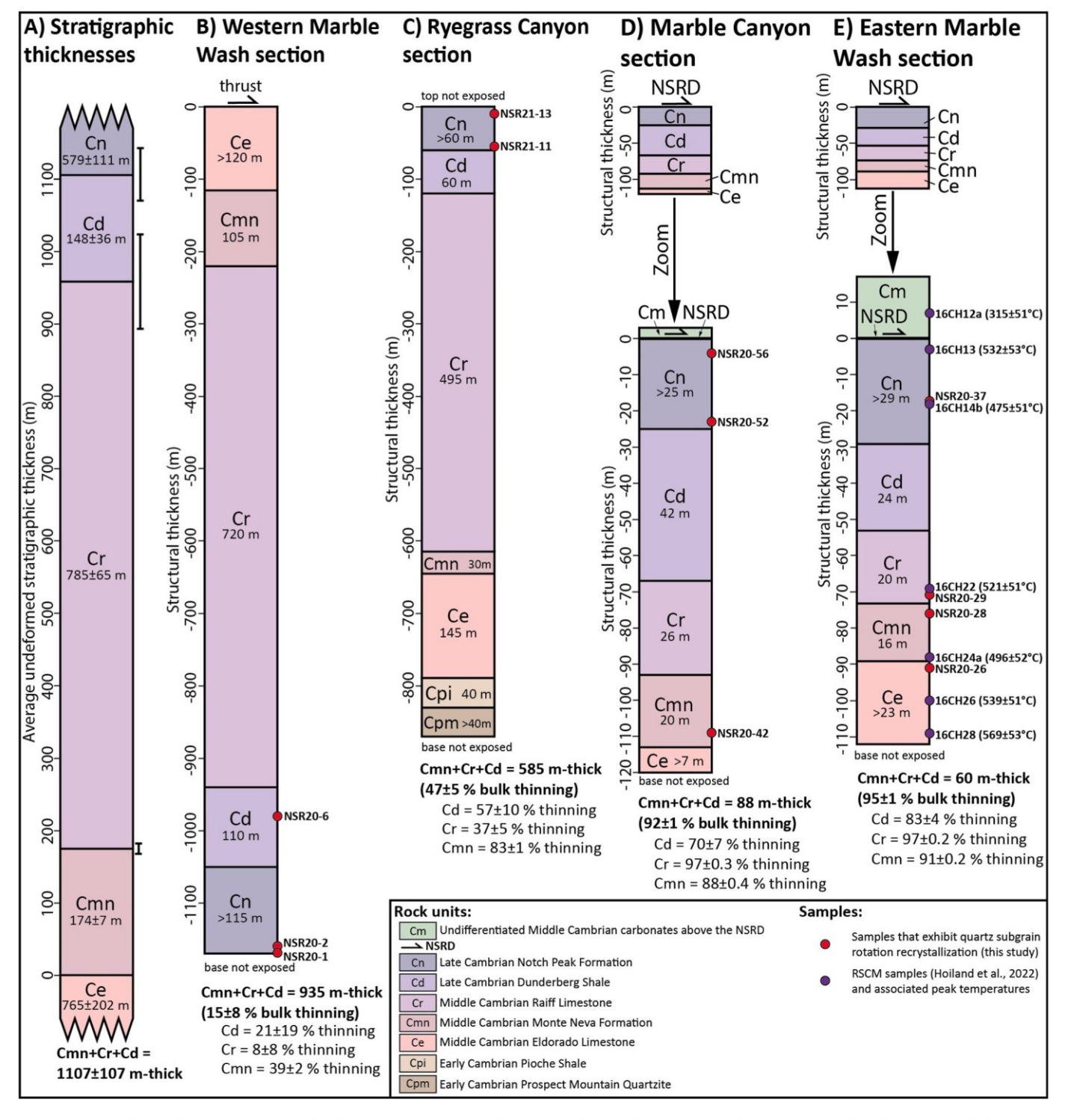


Fig. 12. Stratigraphic thicknesses of unstrained and unmetamorphosed Middle-Late Cambrian carbonate units (column A) compared to the structural thicknesses of strained and metamorphosed Middle-Late Cambrian carbonate units in the NSRD footwall from west to east across the northern part of the Northern Snake Range (columns B-E). A) The mean stratigraphic thicknesses of unstrained and unmetamorphosed Middle-Late Cambrian rock units, based on thicknesses reported in the Schell Creek and Egan Ranges to the west (see text section 4.1 for details). Error bars for measured stratigraphic thicknesses of units Cmn, Cr, and Cd are shown to the right of the upper stratigraphic contact of each unit. B-E) Structural thicknesses of Middle-Late Cambrian rock units measured in the B) Western Marble Wash, C) Ryegrass Canyon, D) Marble Canyon, and E) Eastern Marble Wash sections. Bulk thinning and individual unit thinning percentages are listed below the columns.

respectively, and a total Late Eocene-Late Oligocene extension magnitude of 12.1 ± 2.2 km ($167 \pm 31\%$) (Fig. 15C; Table 2).

This restoration is based on assumption that the low-magnitude bulk thinning in the western part of the range that was accomplished during Late Cretaceous ductile deformation affected all rocks that are presently exposed in the NSRD footwall to the east. This assumption is supported

by observations of inclusion trails preserved in Late Cretaceous metamorphic porphyroblasts in the NSRD footwall in the southeastern part of the range (Miller et al., 1988; Lewis et al., 1999; Cooper et al., 2010B). Alternatively, if we assume no Late Cretaceous bulk thinning, restoration of the thinned units in strain domains 3–5 to their original stratigraphic thicknesses yields a total pre-Late Eocene, NSRD-parallel length

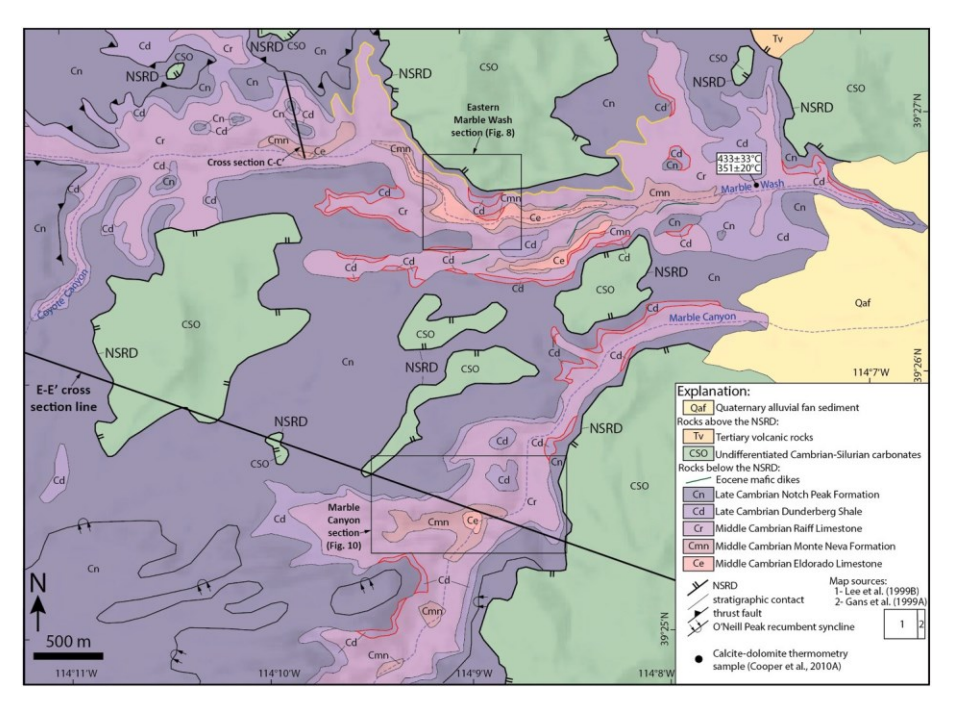


Fig. 13. Geologic map of the eastern portion of Marble Wash and Marble Canyon (compiled from Lee et al., 1999B, and Gans et al., 1999A; map pattern of the O'Neill Peak recumbent syncline is from Wrobel et al., 2021). Contacts bounding megaboudins of the Dunderberg Shale (Cd; n = 22) and Monte Neva Formation (Cmn; n = 2) are highlighted in red. Yellow contacts highlight two places on the northern side of Marble Wash where megaboudins of the Dunderberg Shale are separated by ~1 km lineation-parallel distance. Calcite-dolomite thermometry results from eastern Marble Wash (Cooper et al., 2010A) are shown. (For interpretation of the references to colour in this figure legend, the reader is referred to the Web version of this article.)

of 5.7 \pm 0.9 km. From this, we calculate a total extension magnitude of 13.7 \pm 0.9 km (239 \pm 15%), which represents the maximum possible magnitude of ductile strain in the NSRD footwall during Late Eocene-Late Oligocene extension. However, given the evidence that Late Cretaceous ductile fabrics likely extended across the full width of the range (e.g., Miller et al., 1988), the 12.1 \pm 2.2 km (167 \pm 31%) estimate for Late Eocene-Late Oligocene ductile extension is our preferred estimate.

7. Deformation temperature constraints from quartz recrystallization microstructures and published calcite-dolomite thermometry

The dominant mechanism of dynamic recrystallization of quartz, which can be interpreted from the morphology of recrystallized quartz in thin sections, allows placing approximate constraints on the deformation temperature of ductile deformation (e.g., Law, 2014). In 12 thin sections of Middle-Late Cambrian marbles from the NSRD footwall, we observed evidence for quartz subgrain rotation recrystallization within quartz-rich patches and laminations that are deformed parallel to tectonic foliation (Fig. 16). Subgrain rotation is indicated by an equigranular microtexture of ~30-80 µm-diameter subgrains (e.g., Stipp et al., 2002). We observed subgrain rotation in three samples from the Western Marble Wash section, two from the Ryegrass Canyon section, three from the Marble Canyon section, and four from the Eastern Marble Wash section (Fig. 12). Subgrain rotation recrystallization indicates an approximate deformation temperature range of ~400-550 °C, using the combined ranges estimated by Stipp et al. (2002) and Law (2014). We interpret this temperature range as approximate, as mechanisms of quartz recrystallization can be dependent on several other factors, including strain rate and water content (e.g., Law, 2014). This temperature range is consistent with calcite-dolomite thermometry from the eastern part of Marble Wash (Fig. 13), which yielded deformation temperature estimates of 433 \pm 33 °C for an early phase and 351 \pm 20 °C for a later phase of Late Eocene-Late Oligocene extensional ductile shearing (Cooper et al., 2010A).

8. Discussion

8.1. Comparison of NSRD footwall strain between the northern and southern parts of the Northern Snake Range

Contours of foliation-normal (Z) thinning and lineation-parallel (X) extension from our study of Middle-Late Cambrian marbles in the northern part of the range, combined with similar data measured from the Prospect Mountain Quartzite in the southern part of the range (Lee et al., 1987; Long et al., 2022; Blackford, 2023) (Fig. 4B and C), demonstrates a dramatic eastward increase in ductile strain magnitude in the NSRD footwall and exceptionally high strain along the entire eastern flank of the range. However, the total ductile extension magnitude and the lineation-parallel length of the strain gradient decrease northward. The magnitude of Late Eocene-Late Oligocene subhorizontal ductile extension in the southern part of the range is estimated at 19.1-19.7 km (Lee et al., 1987; Long et al., 2022; Blackford, 2023), which is 1.3-2.0 times greater than the 12.1 \pm 2.2 km of extension that we measured along cross section E-E' in the northern part of the range (Fig. 15C). In the southern part of range, Z thinning increases from 28% at the western limit of Late Eocene-Late Oligocene ductile fabrics to 94% in the eastern part of the range, across a lineation-parallel distance of 20.6 km (Blackford, 2023). However, on our cross section E-E', only a 12 km lineation-parallel distance separates the western limit of Late Eocene-Late Oligocene ductile fabrics (15% Z thinning) and the western limit of strain domain 5 (92% Z thinning) (Fig. 15A).

The Ryegrass Canyon section exhibits lower strain (47% Z thinning) compared to lineation-normal locations ~8–10 km to the NNE (92–95% Z thinning) and ~4 km to the SSW (91% Z thinning), and spatially corresponds with a ~4.5 km eastward swing in the western limit of Late Eocene-Late Oligocene ductile fabrics (Fig. 4). The Ryegrass Canyon section lies within a ~2-3 km-wide (NNE-to-SSW), ~0.4–0.8 km-deep topographic trough in the NSRD (Lee et al., 1999C). We speculate that the anomalously low strain in the Ryegrass Canyon section may be the consequence of restriction of ductile flow of NSRD footwall rocks due to vertical narrowing within this trough.

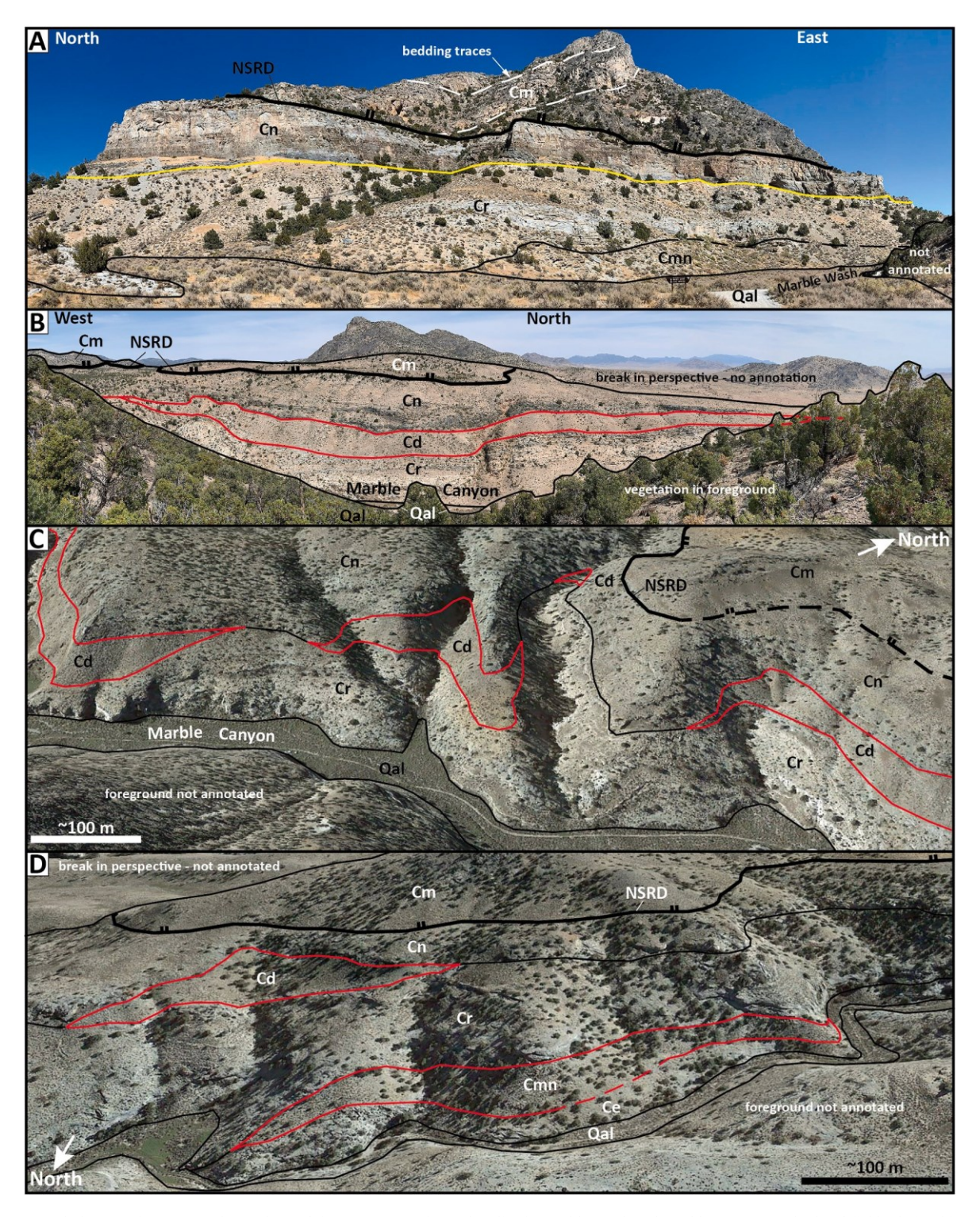


Fig. 14. Annotated photographs (A-B) and Google Earth images (C-D) of megaboudins in Marble Wash and Marble Canyon, and related field relationships (see Fig. 2 for a guide to unit abbreviations). A) View to the NNE of part of the northern side of Marble Wash, where the Raiff Limestone (Cr) and Notch Peak Formation (Cn) are in direct structural contact (highlighted in yellow) for several hundred meters, as a consequence of ~1 km of separation between megaboudins of the Dunderberg Shale (39.44817 °N, 114.15747 °W). B) View to the north of the northern side of Marble Canyon, with a ~1 km-long megaboudin of the Dunderberg Shale (Cd) highlighted in red (the point where the boudin pinches out on the right-hand side is obscured by foreground vegetation) (39.43419 °N, 114.13539 °W). C) Oblique view to the northwest of part of Marble Canyon, with four megaboudins of the Dunderberg Shale (Cd) highlighted in red. D) Oblique view to the southeast of a drainage on the southern side of Marble Wash, with megaboudins of the Monte Neva Formation (Cmn) and Dunderberg Shale (Cd) highlighted in red. (For interpretation of the references to colour in this figure legend, the reader is referred to the Web version of this article.)

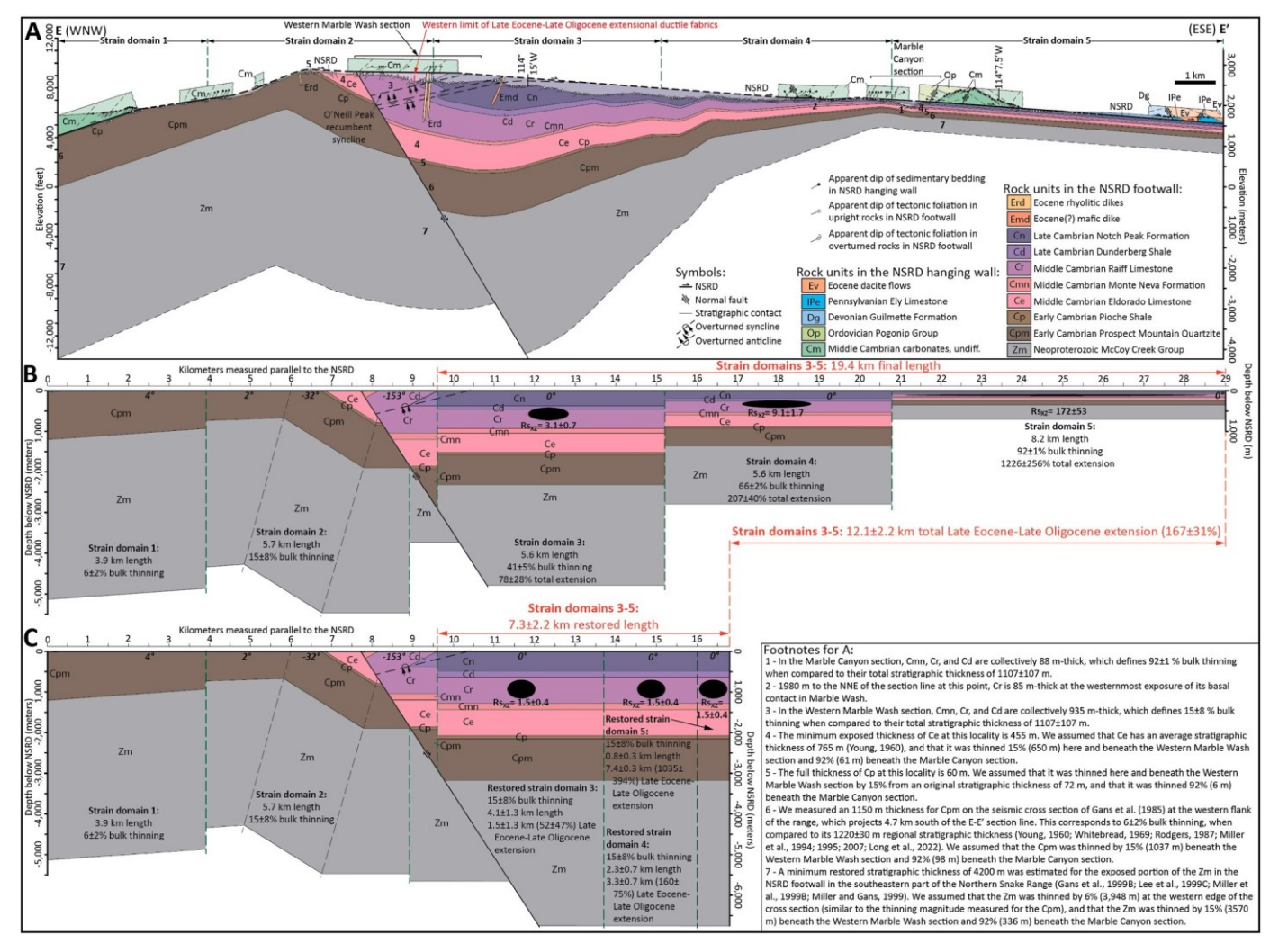


Fig. 15. A) Cross-section E-E' across the northern part of the Northern Snake Range (line of section shown on Fig. 2), which is supported by the mapping of Lee et al., 1999A; 1999B; Gans et al., 1999A, and our measurements proximal to the Western Marble Wash and Marble Canyon sections. The E-E' section line is drafted parallel to the 295°/115° average trend of Late Eocene-Late Oligocene stretching lineations (see Fig. 4A), which is parallel to the direction of ductile stretching of the NSRD footwall. Bold numbers are keyed to footnotes in the lower right-hand part of the figure. B) Five-domain strain model for the NSRD footwall along E-E' (plotted with depth below the NSRD on the vertical axis and distance measured parallel to the NSRD on the horizontal axis), showing the present-day geometry. NSRD-parallel lengths, bulk thinning, extension, and the Rsxz values of strain ellipses are shown for strain domains 3–5 (details in text section 6 and Table 2). Angles listed in italics represent average NSRD footwall cutoff-angles (positive and negative angles correspond with the NSRD cutting down-section and up-section toward the ESE, respectively). C) Restored strain model for the NSRD footwall, with strain domains 3–5 restored to their geometry prior to Late Eocene-Late Oligocene ductile extension (details in text section 6 and Table 2).

8.2. Structural, thermal and geometric factors that promoted development of the extreme strain gradient

Here, we utilize deformation temperatures from the NSRD footwall across the northern part of the range (this study; Cooper et al., 2010A) and published thermochronometry from the NSRD footwall across the central part of the range (Lee and Sutter, 1991; Lee, 1995) to interpret a structural scenario that can explain the origin, geometry and magnitude of the extreme strain gradient along cross section E-E'. This discussion is accompanied by Fig. 17, which illustrates three stages in the progressive ductile shearing of the NSRD footwall along E-E'.

The deformation temperature of ductile shearing within Middle-Late Cambrian marbles in the NSRD footwall across much of the width of the northern part of the range is constrained to an approximate range of $\sim\!400{-}550$ °C, based on our observations of subgrain rotation recrystallization within quartz patches and laminations that are deformed parallel to the Late Eocene-Late Oligocene extensional foliation (Fig. 16). This is consistent with calcite-dolomite thermometry that measured a deformation temperature of 433 \pm 33 °C (Cooper et al.,

2010A) for an early phase of Late Eocene-Late Oligocene ductile extensional shearing in the northeastern part of the range (Figs. 13 and 17A)

Muscovite K-Ar and ⁴⁰Ar/³⁹Ar ages (Lee et al., 1980; Lee and Sutter, 1991) and K-feldspar ⁴⁰Ar/³⁹Ar multi-diffusion domain modeling (Lee, 1995) from samples collected ~10–15 km to the south of E-E' (Fig. 2), which project northward to strain domains 3-5, indicate that NSRD footwall rocks in the eastern part of the range stayed hotter for longer compared to rocks in the western part of the range. Projected K-Ar and ⁴⁰Ar/³⁹Ar muscovite ages demonstrate that NSRD footwall rocks cooled through an estimated closure temperature of ~405 °C (e.g., Harrison et al., 2009) between ~50 and 40 Ma in the western part of strain domain 3, between ~40 and 30 Ma in the eastern part of strain domain 3 and western part of strain domain 4, and between ~30 and 24 Ma in the eastern part of strain domain 4 and strain domain 5 (Figs. 2 and 17) (Lee and Sutter, 1991). K-feldspar 40Ar/39Ar multi-diffusion domain modeling from three samples (KPA2-4) that project northward to strain domains 3 and 4 (Fig. 2) resided at \sim 290–350 °C until as late as \sim 22 Ma (Lee, 1995).

Table 2Data that support the restoration of the finite strain model shown in Fig. 15.

	Modern	Modern	Foliation-	Lineation-	Lineation-	Strain	Strain	Restored	Late Eocene-	Late Eocene-
Strain	WNW-ESE	NSRD- parallel	normal (Z)	normal (Y)	parallel (X)	ellipsoid	ellipsoid	NSRD- parallel	Late Oligocene	Late Oligocene
domain	length (km)	length (km)	shortening (%)	shortening	extension (%)	RsXZ d	RsYZ d	length (km)	extension (km)	extension (%)
1	3.7	3.9	6 ± 2 a	-	-	-	-	-	-	-
2	5.6	5.7	15 ± 8 a	-	-	-	-	-	-	-
3	5.6	5.6	41 ± 5^{b}	3 ± 7 °	78 ± 28	3.1 ± 0.7	1.7 ± 0.02	4.1 ± 1.3	1.5 ± 1.3	52 ± 47
4	5.6	5.6	66 ± 2^{b}	3 ± 7 °	207 ± 40	9.1 ± 1.7	2.9 ± 0.04	2.3 ± 0.7	3.3 ± 0.7	160 ± 75
5	8.2	8.2	92 ± 1 ª	3 ± 7 °	1226 ± 256	172 ± 53	12.2 ± 0.62	0.8 ± 0.3	7.4 ± 0.3	1035 ± 394
Total (3- 5)	19.4	19.4	-	-	-	-	-	7.3 ± 2.2	12.1 ± 2.2	167 ± 31

^a Measured foliation-normal bulk thinning values from unit Cpm (strain domain 1) and units Cmn + Cr + Cd from the Western Marble Wash (strain domain 2) and Marble Canyon sections (strain domain 5); see footnotes 1, 3, and 7 on Fig. 15A for additional details.

The eastward progression of cooling of the NSRD footwall may help explain the genesis of the strain gradient in Middle-Upper Cambrian marbles. Studies of calcite-rich fault rocks have interpreted a ~150–250 °C lower temperature limit for dynamic recrystallization (e. g., Kennedy and White, 2001), and studies of calcite marbles have documented a significant decrease in strength accompanying the initiation of grain boundary sliding and dislocation activity at temperatures as low as ~300 °C (e.g., Rogowitz et al., 2016). Cambrian marbles in the NSRD footwall in the eastern part of the range stayed hot, ductile, and weak for longer, residing at or above ~405 °C until as late as ~24 Ma (Lee and Sutter, 1991) and not cooling through ~250 °C until as late as ~18 Ma (Lee, 1995, sample KPA3). This increase in temperature may have, in part, been the consequence of the eastward elevation of isotherms within subhorizontal rocks in the NSRD footwall due to strain heating (e.g., Pavlis, 1986; England et al., 1992; Nabelek et al., 2010), which is illustrated on Fig. 17. We suggest that strain heating, which scaled with strain magnitude and thus became more significant eastward, may have served as a positive-feedback process that increased the longevity of thermally enhanced ductile weakening of Middle-Late Cambrian marbles in the eastern part of the range. One alternative interpretation is that the eastward increase in temperatures was the result of a pre-extensional eastward dip of NSRD footwall rocks and thus a deeper burial depth along the eastern flank of the range, as originally proposed by Lee and Sutter (1991) and Lee (1995). A third alternative is that strain heating was superimposed on the eastward-dipping footwall rocks. Regardless of the specific geometric scenario, marble units in the NSRD footwall experienced a longer ductile strain history in the eastern part of the range, which can account for the dramatic eastward increase in stretching and thinning.

Fig. 17 shows one possible geometric scenario for generating the extreme ductile strain gradient in the NSRD footwall along E-E'. We interpret that the brittle, top-down-to-ESE NSRD rooted eastward below the 300 °C isotherm into a moderately east-dipping, top-down-to-ESE, simple shear-dominant ductile shear zone that cuts obliquely down-section eastward across Cambrian and Neoproterozoic rocks. Below and to the west of this top-down-to-ESE ductile shear zone, a region of low-strain, pure shear-dominant ductile stretching is shown below the ~300 °C isotherm, extending to the observed western limit of Late Eocene-Late Oligocene ductile fabrics (Fig. 17A). This geometry results in an eastward transition from pure shear-dominant deformation to

simple shear-dominant deformation across the NSRD footwall. This scenario is supported by quartz crystallographic fabrics from the NSRD footwall in the southern part of the range, which transition west-to-east across the range from symmetric to strongly asymmetric and have been interpreted to represent an eastward transition from pure shear-dominant to simple shear-dominant deformation (Lee et al., 1987; G´ebelin et al., 2011; 2015).

The combination of the strong asymmetry in the strain gradient in the NSRD footwall, exceptionally high strain along the eastern flank of the range, a nearly ubiquitous top-to-ESE shear-sense in the eastern part of the range, and ⁴⁰Ar/³⁹Ar and K-Ar ages that record an eastward progression of cooling indicate: A) prolonged residence time at higher temperatures along the eastern flank of the range compared to the western flank, which aided the development of the extreme strain gradient, and B) differential unroofing of NSRD footwall rocks that were deformed by a top-down-to-ESE, simple shear-dominant ductile shear zone that dipped steeper to the east than bedding (e.g., Lee et al., 1987; Lee, 1995).

9. Conclusions

- 1) In the northern part of the Northern Snake Range, Middle-Late Cambrian marbles in the NSRD footwall were ductilely stretched and thinned during Late Eocene-Late Oligocene ductile extension, with thinning increasing eastward from ~15-21% to ~92–95% across a 12 km lineation-parallel distance. This extreme thinning generated pervasive linear-planar ductile fabrics and 100-500 mlong, 15-25 m-thick megaboudins of calcareous schist that are separated by as much as 1 km. Lineation-parallel extension increases eastward to 1226 ± 256%. Late Eocene-Late Oligocene ductile shearing extended the eastern portion of the NSRD footwall from a 7.3 ± 2.2 km initial length to a 19.4 km final length, corresponding to 12.1 ± 2.2 km of total ductile extension (167 ± 31%).
- 2) Combining our strain data with similar data from the southern part of the range demonstrates that the full exposed extent of the NSRD footwall is characterized by a dramatic west-to-east strain gradient and extremely high strain along the eastern flank of the range. A longer ductile strain history and a prolonged residence time at higher temperatures on the eastern side of the range, which was likely facilitated by strain heating that scaled eastward with strain magnitude and/or a possible eastward increase in burial depth,

b Determined by interpolation between 15 ± 8% bulk thinning measured in strain domain 2 and 92 ± 1% bulk thinning measured in strain domain 5.

^c Assumed $3 \pm 7\%$ Y shortening during Late Eocene-Late Oligocene ductile strain, which is the mean $(\pm 1\sigma)$ of 11 strain ellipsoids from the NSRD footwall in the southern part of the range (Lee et al., 1987; their Table 1), calculated by restoring each ellipsoid to a sphere with the same volume.

^d Strain ellipsoid X extension values and Rs ratios were calculated to match the constrained Z shortening and Y shortening values, by restoring the ellipsoid to a sphere with the same volume. Reported errors were calculated using the error ranges on Z shortening and Y shortening.

e Restored NSRD-parallel lengths for strain domains 3–5 were calculated by restoring their strain ellipsoids to match the 15 ± 8% bulk Z thinning from strain domain

^{2.} Assuming 3 ± 7% Y shortening, this involved restoration to a strain ellipsoid with an RsXZ of 1.5 ± 0.4, an RsYZ of 1.1 ± 0.02, and 24 ± 21% X extension.

f Calculated by subtracting the restored NSRD-parallel length from the modern NSRD-parallel length.

g Calculated using the error ranges of Late Eocene-Late Oligocene extension and restored NSRD-parallel length.

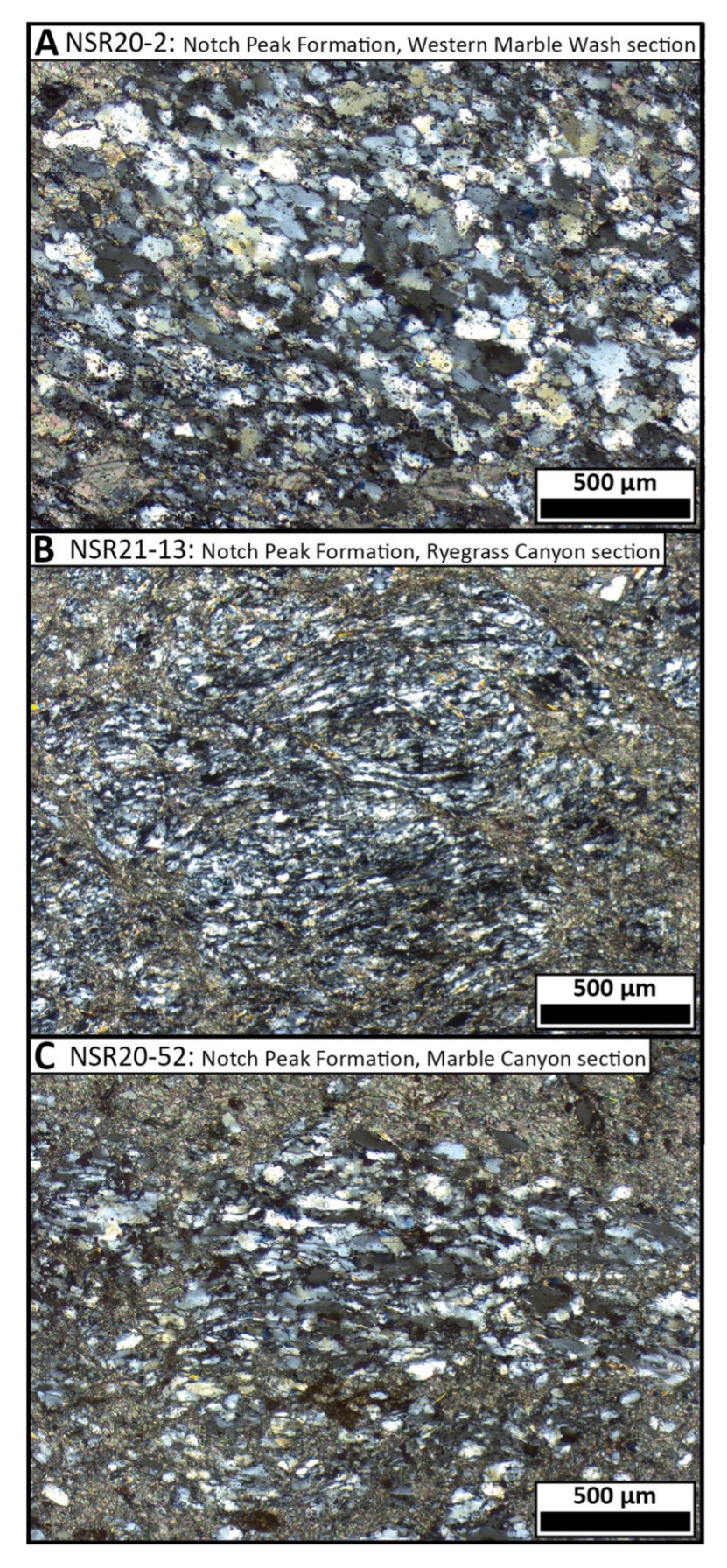


Fig. 16. A-C) Photomicrographs (taken in cross-polarized light) of representative examples of subgrain rotation recrystallization of quartz in foliation-normal, lineation-parallel thin sections of Middle-Late Cambrian marbles, as indicated by equigranular textures of \sim 30–80 μ m-diameter quartz subgrains.

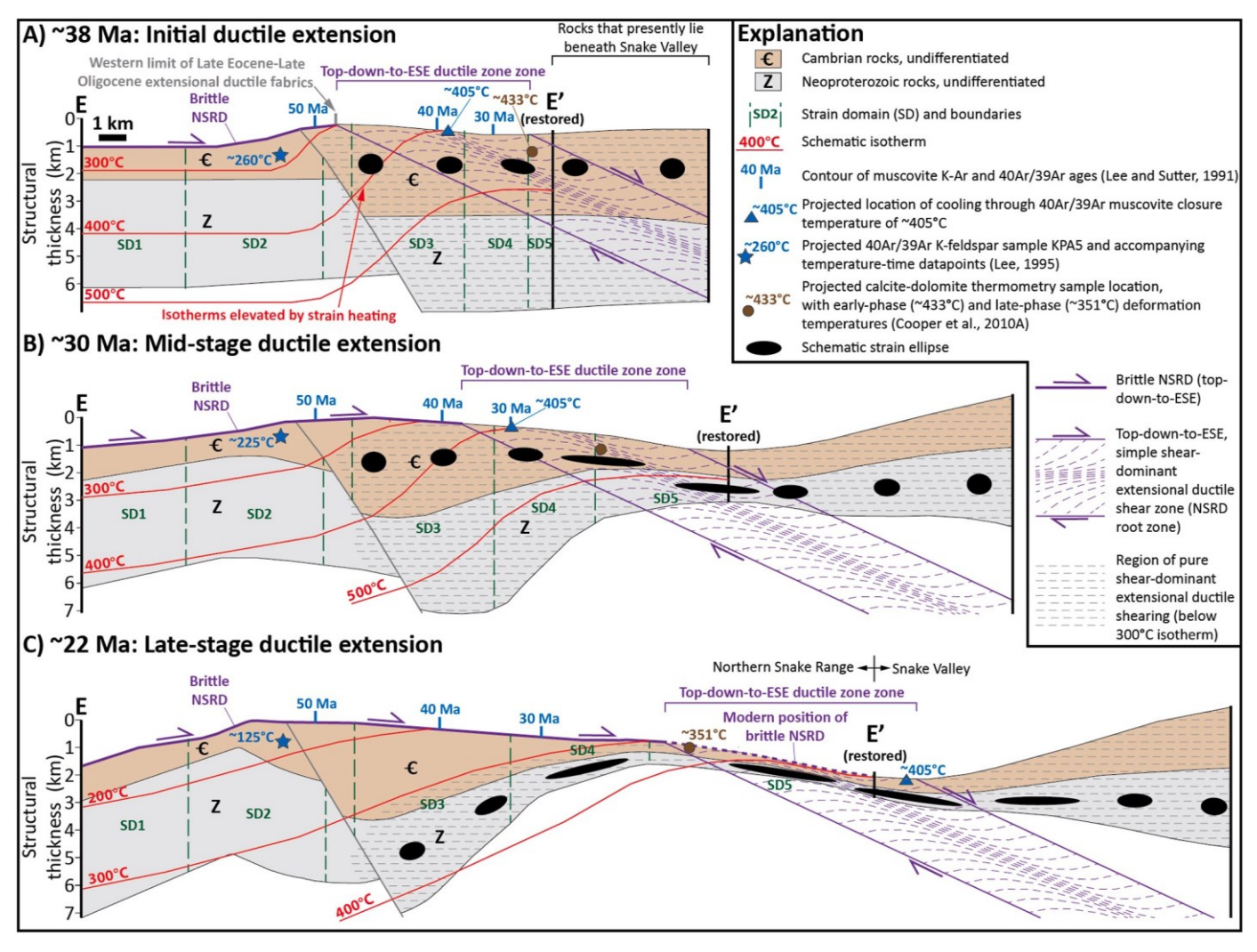


Fig. 17. Schematic cross section diagrams illustrating three stages in the progressive ductile extension of the Northern Snake Range d`ecollement (NSRD) footwall along cross section E-E', including: A) the initiation of ductile extension at ~38 Ma, B) mid-stage ductile extension at ~30 Ma, and C) late-stage ductile extension at ~22 Ma (timing constraints from Lee et al., 2017). For simplicity, rocks in the NSRD hanging wall are not shown, and no attempt was made to account for the evolution of dip angles as a consequence of isostatic rebound during extension. Schematic isotherms are supported by the temperature-time history of projected ⁴⁰Ar/³⁹Ar K-feldspar sample KPA5 in the western part of the range (sample location shown on Fig. 2) from Lee (1995), the contours of K-Ar and ⁴⁰Ar/³⁹Ar muscovite ages across the central part of the range from Lee and Sutter (1991) (Fig. 2), which record the timing of cooling through a closure temperature of ~405 °C (e.g., Harrison et al., 2009), the ~400–550 °C range of deformation temperatures from our quartz recrystallization observations across the eastern two-thirds of the range, and calcite-dolomite thermometry from Cooper et al. (2010A) from the eastern part of the range (~433 °C and ~351 °C during early and late phases of Late Eocene-Late Oligocene extensional ductile shearing, respectively) (sample location shown on Fig. 13). The cross sections show an interpreted scenario in which strain into an east-dipping, top-down-to-ESE, simple shear-dominant ductile shear zone that cuts obliquely down-section eastward across Cambrian and Neoproterozoic rocks. To the west of this ductile shear zone, a region of pure shear-dominant ductile stretching is shown below the ~300 °C isotherm, extending to the observed western limit of Late Eocene-Late Oligocene extensional ductile fabrics. Pure shear-dominant stretching is also schematically shown for rocks that lie to the east of the simple shear-dominant ductile shear zone.

promoted the development of the extreme strain gradient in the NSRD footwall

Author statement

Sean Long: Conceptualization, Methodology, Formal analysis, Investigation, Writing – original draft, Writing – Review and editing, Visualization, Funding Acquisition. **Jeffrey Lee:** Conceptualization, Writing – original draft, Writing- Review and editing, Visualization, Funding Acquisition. **Nolan Blackford:** Writing – Review and Editing.

Declaration of competing interest

The authors declare that they have no known competing financial

interests or personal relationships that could have appeared to influence the work reported in this paper.

Data availability

All data used for this research is included in the manuscript.

Acknowledgements

This work was supported by National Science Foundation grants EAR-2022973 awarded to Sean Long and EAR-2022979 awarded to Jeffrey Lee. We thank two anonymous reviewers for constructive reviews that improved the manuscript.

References

- Allmendinger, R.W., 1992. Fold and thrust tectonics of the western United States exclusive of the accreted terranes. In: Burchfiel, B.C., Lipman, P.W., Zoback, M.L. (Eds.), Geology of North America, Volume G-3: the Cordilleran Orogen: Conterminous USA. Geological Society of America, Boulder, Colorado, pp. 583–607.
- Anderson, R.E., Zoback, M.L., Thompson, G.A., 1983. Implications of selected subsurface data on the structural form and evolution of some basins in the northern Basin and Range Province, Nevada and Utah. Geol. Soc. Am. Bull. 94, 1055–1072.
- Armstrong, R.L., 1972. Low-angle (denudation) faults, hinterland of the Sevier orogenic belt, eastern Nevada and western Utah. Geol. Soc. Am. Bull. 83, 1729–1754.
- Armstrong, R.L., Hansen, E., 1966. Cordilleran infrastructure in the eastern Great Basin. Am. J. Sci. 254, 112–127.
- Axen, G.J., Lewis, K.J., Burke, K.J., Sleeper, K.G., Fletcher, J.M., 1988. Tertiary extension in the Pioche area, Nevada. In: Weide, D.L., Faber, M.L. (Eds.), This Extended Land, Geological Journeys in the Southern Basin and Range, Cordilleran Section Field Trip Guidebook. Geological Society of America, Las Vegas, Nevada, pp. 3-5.
- Axen, G.J., Taylor, W.J., Bartley, J.M., 1993. Space-time patterns and tectonic controls of Tertiary extension and magmatism in the Great Basin of the western United States. Geol. Soc. Am. Bull. 105, 56–76. https://doi.org/10.1130/0016-7606(1993) 105~0036:STPATC>2.3.CO:2.
- Bailey, C.M., Eyster, E.L., 2003. General shear deformation in the Pinalen o Mountains metamorphic core complex, Arizona. J. Struct. Geol. 25 (11), 1883–1892. https://doi.org/10.1016/S0191-8141(03)00044-0.
- Bartley, J.M., Wernicke, B.P., 1984. The Snake Range d'ecollement interpreted as a major extensional shear zone. Tectonics 3, 647–657.
- Barton, M.D., 1990. Cretaceous magmatism, metamorphism, and metallogeny in the east-central Great Basin. In: Anderson, J.L. (Ed.), The Nature and Origin of Cordilleran Magmatism, 174. Geological Society of American Memoir, pp. 283–302. https://doi.org/10.1130/MEM174-p283.
- Barton, M.D., Battles, D.A., Debout, G.E., Capo, R.C., Christensen, J.N., Davis, S.R., Hanson, R.B., Michelsen, C.J., Trim, H.E., 1988. Mesozoic contact metamorphism in the western United States. In: Ernst, W.G. (Ed.), Metamorphism and Crustal Evolution, Western United States, Rubey Volume VII. Prentice-Hall, Englewood Cliffs, New Jersey, pp. 110–178.
- Best, M.G., Barr, D.L., Christiansen, E.H., Gromme, S., Deino, A.L., Tingey, D.G., 2009. The Great Basin Altiplano during the middle Cenozoic ignimbrite flareup: insights from volcanic rocks. Int. Geol. Rev. 51, 589–633. https://doi.org/10.1080/00206810902867690.
- Blackford, N.R., 2023. The Evolution of the Nevadaplano from Construction to Dismemberment: Investigations of Thermal Conditions, Strain Distribution, and Fabric Intensity in Eastern Nevada and Western Utah [Ph.D. Dissertation]. tables, 34 figures,. Washington State University, Pullman, Washington, p. 12, 251, 1 plate.
- Blackford, N.R., Long, S.P., Stout, A.J., Rodgers, D.W., Cooper, C.M., Kramer, K., Di Fiori, R.V., Soignard, E., 2022. Late Cretaceous upper-crustal thermal structure of the Sevier hinterland: implications for the geodynamics of the Nevadaplano. Geosphere 18, 183–210. https://doi.org/10.1130/GES02386.1.
- Buck, W.R., 1988. Flexural rotation of normal faults. Tectonics 7, 9595–9973. Burchfiel, B.C., Cowan, D.S., Davis, G.A., 1992. Tectonic overview of the Cordilleran
- orogen in the western United States. In: Burchfiel, B.C., Lipman, P.W., Zoback, M.L. (Eds.), Geology of North America, Volume G-3: the Cordilleran Orogen:
 Conterminous USA, Geological Society of America, Boulder, Colorado, pp. 407–480.
- Camilleri, P.A., Chamberlain, K.R., 1997. Mesozoic tectonics and metamorphism in the Pequop Mountains and Wood Hills region, northeast Nevada: implications for the architecture and evolution of the Sevier orogen. Geol. Soc. Am. Bull. 109, 74–94. https://doi.org/10.1130/0016-7606 (1997)109 < 0074:MTAMIT > 2.3.CO;2.
- Cassel, E.J., Breecker, D.O., Henry, C.D., Larson, T.E., Stockli, D.F., 2014. Profile of a paleo-orogen: high topography across the present-day Basin and Range from 40 to 23 Ma. Geology 42, 1007–1010. https://doi.org/10.1130/G35924.1.
- Chapman, J.B., Ducea, M.N., DeCelles, P.G., Profeta, L., 2015. Tracking changes in crustal thickness during orogenic evolution with Sr/Y: an example from the North American Cordillera. Geology 43, 919–922. https://doi.org/10.1130/G36996.1.
- Coney, P.J., 1974. Structural analysis of the Snake Range d´ecollement, east-central Nevada. Geol. Soc. Am. Bull. 85, 973–978. https://doi.org/10.1130/0016-7606 (1974)85<973:SAOTSR>2.0.CO;2.
- Coney, P.J., Harms, T., 1984. Cordilleran metamorphic core complexes: Cenozoic extensional relics of Mesozoic compression. Geology 12, 550–554.
- Coogan, J.C., 1992. Thrust Systems and Displacement Transfer in the Wyoming-Idaho-Utah Thrust Belt [Ph.D. Dissertation]. report. University of Wyoming, Laramie, Wyoming, p. 240, 55 figs., 2 plates.
- Cooper, F.J., Platt, J.P., Platzman, E.S., Grove, M.J., Seward, G., 2010A. Opposing shear senses in a subdetachment mylonite zone: implications for core complex mechanics. Tectonics 29, TC4019. https://doi.org/10.1029/2009TC002632.
- Cooper, F.J., Platt, J.P., Anczkiewicz, R., Whitehouse, J., 2010B. Footwall dip of a core complex detachment fault: thermobarometric constraints from the northern Snake Range (Basin and Range, USA). J. Metamorph. Geol. 28, 997–1020. https://doi.org/ 10.1111/j.1525-1314.2010.00907.x.
- Cordilleran Metamorphic Core Complexes. In: Crittenden Jr., M.D., Coney, P.J., Davis, G. H. (Eds.), Geological Society of America Memoir 153, 490. https://doi.org/10.1130/MEM153-p485 p., doi:
- Davis, G.H., 1983. Shear-zone model for the origin of metamorphic core complexes Geology 11, 342–347.
- DeCelles, P.G., 2004. Late Jurassic to Eocene evolution of the Cordilleran thrust belt and foreland basin system, western USA. Am. J. Sci. 304, 105–168. https://doi.org/ 10.2475/ajs.304.2.105.

- DeCelles, P.G., Coogan, J.C., 2006. Regional structure and kinematic history of the Sevier fold-and-thrust belt, central Utah. Geol. Soc. Am. Bull. 118, 841–864.
- Dechert, C.P., 1967. Bedrock Geology of the Northern Schell Creek Range, White Pine County, Nevada [Ph.D. Dissertation]. University of Washington, Seattle, Washington, p. 266.
- Dickinson, W.R., 2002. The Basin and Range province as a composite extensional domain. Int. Geol. Rev. 44, 1–38. https://doi.org/10.2747/0020-6814.44.1.1.
- Dickinson, W.R., Snyder, W.S., 1978. Plate tectonics of the Laramide orogeny. In:
 Matthews III, V. (Ed.), Laramide Folding Associated with Basement Block Faulting in
 the Western United States, 151. Geol. Soc. Amer. Memoir, pp. 355–366.
- Drewes, H., 1967. Geology of the Connors Pas Quadrangle, Schell Creek Range, East-Central
- Druschke, P., Hanson, A.D., Wells, M.L., 2009. Structural, stratigraphic, and geochronologic evidence for extension predating Palaeogene volcanism in the Sevier hinterland, east-central Nevada. Int. Geol. Rev. 51, 743–775. https://doi.org/ 10.1080/00206810902917941.
- England, P., LeFort, P., Molnar, P., P*echer, A., 1992. Heat sources for Tertiary metamorphism and anatexis in the Annapurna-Manaslu region, central Nepal. J. Geophys. Res. V. 97, 2107–2128.
- Evans, S.L., Styron, R.H., van Soest, M.C., Hodges, K.V., Hanson, A.D., 2015. Zircon and apatite (U-Th)/He evidence for Paleogene and Neogene extension in the southern Snake range, Nevada, USA. Tectonics 34, 2142–2164. https://doi.org/10.1002/2015TC003913.
- Fritz, W.H., 1968. Geologic map and sections of the southern cherry Creek and northern egan ranges, white pine county, Nevada. Nevada Bur. Mines and Geol. Map 35 scale 1:62,500, 1 plate.
- Gans, P.B., 1987. An open-system, two-layer crustal stretching model for the eastern Great Basin. Tectonics 6, 1–12. https://doi.org/10.1029/TC006i001p00001.
- Gans, P.B., Miller, E.L., 1983. Style of mid-Tertiary extension in east-central Nevada. In: Gurgel, K.D. (Ed.), Geologic Excursions in the Overthrust Belt and Metamorphic Core Complexes of the Intermountain Region, 59. Utah Geol. Mineral Surv. Spec. Studies, pp. 107–160.
- Gans, P.B., Miller, E.L., McCarthy, J., Oldcott, M.L., 1985. Tertiary extensional faulting and evolving ductile-brittle transition zones in the northern Snake Range and vicinity: new insights from seismic data. Geology 13, 189–193.
- Gans, P.B., Mahood, G.A., Schermer, E., 1989. Synextensional magmatism in the Basin and range province: a case study from the eastern Great Basin. Geol. Soc. Am. Spec. Pap. 223, 53.
- Gans, P.B., Miller, E.L., Lee, J., 1999A. Geologic map of the spring mountain quadrangle, Nevada and Utah, 1 sheet, 1:24,000-scale Nevada Bur. Mines Geol. Field Studies Map ES. 18 12
- Gans, P.B., Miller, E.L., Huggins, C.C., Lee, J., 1999B. Geologic map of the Little Horse Canyon quadrangle, Nevada and Utah. Nevada Bur. Mines Geol. Field Studies Map FS-20, 1 sheet, 1:24,000-scale, 12 p.
- Gans, P.B., Seedorff, E., Fahey, P.L., Hasler, R.W., Maher, D.J., Jeanne, R.A., Shaver, S.A., 2001. Rapid Eocene extension in the robinson district, white pine county, Nevada: constraints from ⁴⁰Ar/³⁹Ar dating. Geology 29, 475–487.
- G'ebelin, A., Mulch, A., Teyssier, C., Heizler, M., Vennemann, T., Seaton, N.C.A., 2011. Oligo-Miocene extensional tectonics and fluid flow across the northern Snake Range detachment system, Nevada. Tectonics 30, TC5010. https://doi.org/10.1029/ 2010TC002797.
- G'ebelin, A., Teyssier, C., Heizler, M.T., Mulch, A., 2015. Meteoric water circulation in a rolling-hinge detachment system (northern Snake Range core complex, Nevada). GSA Bulletin 127, 149–161. https://doi.org/10.1130/B31063.1 v.
- Gessner, K., Ring, U., Johnson, C., Hetzel, R., Passchier, C.W., Gungor, T., 2001. An active bivergent rolling-hinge detachment system: central Menderes metamorphic core complex in western Turkey. Geology 29, 611–614. https://doi.org/10.1130/0091-7613(2001)029<0611:AABRHD>2.0.CO;2.
- Gottlieb, E.S., Miller, E.L., Valley, J.W., Premo, W.R., Fisher, C.M., Vervoort, J.D., Kitajima, K., 2022. Zircon petrochronology of cretaceous cordilleran interior granites of the Snake range and kern mountains, Nevada, USA. In: Craddock, J.P., Malone, D.H., Foreman, B.Z., Konstantinou, A. (Eds.), Tectonic Evolution of the Sevier-Laramide Hinterland, Thrust Belt, and Foreland, and Postorogenic Slab Rollback (180–20 Ma). Geol. Soc. Amer. Spec. https://doi.org/10.1130/2022.2555 (02. Paper 555.
- Greene, D.C., 2014. The Confusion Range, west-central Utah: fold-thrust deformation and a western Utah thrust belt in the Sevier hinterland. Geosphere 10, 148–169. https://doi.org/10.1130/GES00972.1.
- Hallett, B.W., Spear, F.S., 2014. The P-T history of anatectic pelites of the northern East Humboldt Range, Nevada: evidence for tectonic loading, decompression, and anatexis. J. Petrol. 55, 3–36. https://doi.org/10.1093/petrology/egt057.
- Harrison, T.M., Celerier, J., Aikman, A.B., Hermann, J., Heizler, M.T., 2009. Diffusion of ⁴⁰Ar in muscovite. Geochem. Cosmochim. Acta 73 (4), 1039–1051. https://doi.org/ 10.1016/j.gca.2008.09.03.
- Henry, C.D., John, D.A., 2013. Magmatism, ash-flow tuffs, and calderas of the ignimbrite flareup in the western Nevada volcanic field, Great Basin, USA. Geosphere 9, 951–1008. https://doi.org/10.1130/GES00867.1.
- Henry, C.D., McGrew, A.J., Colgan, J.P., Snoke, A.W., Brueseke, M.E., 2011. Timing, distribution, amount, and style of Cenozoic extension in the northern Great Basin. In: Lee, J., Evans, J.P. (Eds.), Geologic Field Trips to the Basin and Range, Rocky Mountains, Snake River Plain, and Terranes of the U.S. Cordillera. Geol. Soc. Amer. Field Guide 21. Geological Society of America. Boulder, CO, pp. 27–66.
- Hoiland, C.W., Hourigan, J., Miller, E.L., 2022. Evidence for large departures from lithostatic pressure during Late Cretaceous metamorphism in the northern Snake Range metamorphic core complex, Nevada. In: Craddock, J.P., Malone, D.H., Foreman, B.Z., Konstantinou, A. (Eds.), Tectonic Evolution of the Sevier-Laramide

- Hinterland, Thrust Belt, and Foreland, and Postorogenic Slab Rollback (180–20 Ma), 555. Geol. Soc. Amer. Spec. Paper, p. 27.
- Hose, R.K., Blake Jr., M.C., 1976. Geology and mineral resources of white pine county, Nevada, 250,000-scale Nevada Bur. Mines Geol. Bull. 85 (1), 32.
- Huggins, C.C., 1990. Nature and Timing of Metamorphism in the Smith Creek Area, Northern Snake Range, Nevada [M.S. Thesis]. report. Stanford University, Palo Alto, California, p. 92.
- Huggins, C.C., Wright, J.E., 1989. Superimposed cretaceous and tertiary metamorphism in the northern Snake range, Nevada. Geol. Soc. America Abstr. Prog. 21, A95.
- Humphreys, E.D., 1995. Post-Laramide removal of the Farallon slab, western United States. Geology 23, 987–990.
- Jessup, M.J., Law, R.D., Searle, M.P., Hubbard, M.S., 2006. Structural Evolution and Vorticity of Flow during Extrusion and Exhumation of the Greater Himalayan Slab, Mount Everest Massif, Tibet/Nepal: implications for orogen-scale flow partitioning. In: Law, R.D., Searle, M.P., Godin, L. (Eds.), Channel Flow, Ductile Extrusion and Exhumation in Continental Collision Zones, 268. Geol. Soc., London, Spec. Publ., pp. 379–413
- Johnston, S.M., 2000. Normal Faulting in the Upper Plate of a Metamorphic Core Complex, Northern Snake Range, Nevada [M.S. Thesis]. report. Stanford University, Palo Alto, California, p. 60.
- Kennedy, L.A., White, J.C., 2001. Low-temperature recrystallization in calcite: mechanisms and consequences. Geology 29, 1027–1030. https://doi.org/10.1130/ 0091-7613(2001)029%3C1027:LTRICM%3E2.0.CO;2.
- Kenney, M., 2013. Intrusive and deformational histories of the footwall rocks in the central part of the northern Snake Range, Nevada. In: Varga, R.J. (Ed.), Proceedings of the 26th Annual Keck Research Symposium in Geology, Keck Geology Consortium, 26. Pomona College, pp. 201–206.
- Law, R.D., 2014. Deformation thermometry based on quartz c-axis fabrics and recrystallization microstructures: a review. J. Struct. Geol. 66, 129–161. https://doi. org/10.1016/j.jsg.2014.05.023.
- Lee, J., 1990. Structural Geology and ⁴⁰Ar/³⁹Ar Thermochronology in the Northern Snake Range Metamorphic Core Complex, Nevada [PhD Dissertation]. report. Stanford University, Palo Alto, California, p. 184.
- Lee, J., 1995. Rapid uplift and rotation of mylonitic rocks from beneath a detachment fault: insights from potassium feldspar 40Ar/39Ar thermochronology, northern Snake Range, Nevada. Tectonics 14, 54–77.
- Lee, J., Sutter, J.F., 1991. Incremental ⁴⁰Ar/³⁹Ar thermochronology of mylonitic rocks from the northern Snake Range, Nevada. Tectonics 10, 77–100.
- Lee, D.E., Marvin, R.F., Stern, T.W., Peterman, Z.E., 1970. Modification of Potassium-Argon Ages by Tertiary Thrusting in the Snake Range, White Pine County, Nevada. U.S. Geol. Surv. Prof. Paper 700-D, p. D92. -DJ02.
- Lee, D.E., Marvin, R.F., Mehnert, H.H., 1980. A Radiometric Age Study of Mesozoic-Cenozoic Metamorphism Is Eastern White Pine County, Nevada and Nearby Utah. USGS Prof, pp. 17–28. Paper 1158-C.
- Lee, J., Miller, E.L., Sutter, J.F., 1987. Ductile strain and metamorphism in an extensional tectonic setting: a case study from the northern Snake Range, Nevada, USA. In: Coward, M.P., Dewey, J.F., Hancock, P.L. (Eds.), Continental Extensional Tectonics, 28. Geol. Soc. London Spec. Publ., pp. 267–298
- Lee, J., Gans, P.B., Miller, E.L., 1999A. Geologic map of the third butte east quadrangle, Nevada. Nevada bur. Mines Geol. Field Studies Map FS-16 (1 sheet), 1:24,000-scale.
- Lee, J., Gans, P.B., Miller, E.L., 1999B. Geologic map of the mormon jack pass quadrangle, Nevada. Nevada Bur. Mines Geol. Field Studies Map FS- 17 (1 sheet), 1: 24 000-scale
- Lee, J., Miller, E.L., Gans, P.B., Huggins, C.C., 1999C. Geologic map of the mount morial quadrangle, Nevada, 1 sheet, 1:24,000-scale Nev. Bur. Mines Geol. Field Studies Map FS-19 12.
- Lee, J., Blackburn, T., Johnston, S., 2017. Timing of mid-crustal ductile extension in the northern Snake Range metamorphic core complex, Nevada: evidence from U/Pb zircon ages. Geosphere 13, 439–459. https://doi.org/10.1130/GES01429.1.
- Lewis, C.J., Wernicke, B.P., Selverstone, J., Bartley, J.M., 1999. Deep burial of the footwall of the northern Snake Range decollement, Nevada. Geol. Soc. Am. Bull. 111, 30, 51
- Lister, G.S., Davis, G.A., 1989. The origin of metamorphic core complexes and detachment faults during Tertiary continental extension in the northern Colorado River region, USA. J. Struct. Geol. 11, 65–94. https://doi.org/10.1016/0191-8141 (89)90036-9.
- Lister, G., Banga, G., Feenstra, A., 1984. Metamorphic core complexes of the cordilleran type in the cyclades, aegean sea, Greece. Geology 12, 221–225. https://doi.org/ 10.1130/0091-7613(1984)12<221:MCCOCT>2.0.CO;2.
- Long, S.P., 2012. Magnitudes and spatial patterns of erosional exhumation in the Sevier hinterland, eastern Nevada and western Utah, USA: insights from a Paleogene paleogeologic map. Geosphere 8, 881–901. https://doi.org/10.1130/GES00783.1.
- Long, S.P., 2015. An upper-crustal fold province in the hinterland of the Sevier orogenic belt, eastern Nevada, USA: a Cordilleran Valley and Ridge in the Basin and Range. Geosphere 11, 404–424. https://doi.org/10.1130/GES01102.1.
- Long, S.P., 2019. Geometry and magnitude of extension in the Basin and Range Province (39°N), California, Nevada, and Utah, USA: constraints from a province-scale cross section. Geol. Soc. Am. Bull. 131, 99–119. https://doi.org/10.1130/B31974.1.
- Long, S.P., Heizler, M.T., Thomson, S.N., Reiners, P.W., Fryxell, J.E., 2018. Rapid Oligocene to early Miocene extension along the Grant Range detachment system, eastern Nevada, USA.: insights from multi-part cooling histories of footwall rocks. Tectonics 37, 4752–4779. https://doi.org/10.1029/2018TC005073.
- Long, S.P., Lee, J., Blackford, N.R., 2022. The low-angle breakaway system for the northern Snake range d'ecollement in the Schell Creek and Duck Creek ranges, eastern Nevada, USA: implications for displacement magnitude. Geosphere 18 (4), 1194–1222. https://doi.org/10.1130/GES02482.1.

- Lund-Snee, J.E., Miller, E.L., 2022. Magmatism, migrating topography, and the transition from Sevier shortening to Basin and Range extension, western United States. In: Craddock, J.P., Malone, D.H., Foreman, B.Z., Konstantinou, A. (Eds.), Tectonic Evolution of the Sevier-Laramide Hinterland, Thrust Belt, and Foreland, and Postorogenic Slab Rollback (180–20 Ma). Geol. Soc. Amer. Spec, p. 23. https://doi. org/10.1130/2021.2555(13. Paper 555.
- Malavieille, J., 1987. Extensional shearing deformation and kilometer-scale "a"-type folds in a Cordilleran metamorphic core complex (Raft River Mountains, northwestern Utah). Tectonics 6 (4), 423–448.
- McGrew, A.J., 1993. The origin and evolution of the southern Snake Range Decollement, east central Nevada. Tectonics 12, 21–34. https://doi.org/10.1029/92TC01713 v.
- McGrew, A.J., Peters, M.T., Wright, J.E., 2000. Thermobarometric constraints on the tectonothermal evolution of the East Humboldt Range metamorphic core complex, Nevada. Geol. Soc. Am. Bull. 112, 45–60. https://doi.org/10.1130/0016-7606 (2000)112<45:TCOTTE>2.0.CO;2.
- Miller, C.F., Bradfish, L.J., 1980. An inner Cordilleran belt of muscovite-bearing plutons. Geology 8 (9), 412–416.
- Miller, E.L., Gans, P.B., 1989. Cretaceous crustal structure and metamorphism in the hinterland of the Sevier thrust belt, western US Cordillera. Geology 17, 59–62. https://doi.org/10.1130/0091-7613(1989)017<0059:CCSAMI>2.3.CO;2.
- Miller, E.L., Gans, P.B., 1999. Geologic map of the Cove quadrangle, Nevada and Utah. Nevada Bur. Mines Geol. Field Studies Map 22, 12 scale 1:24,000, 1 sheet.
- Miller, E.L., Gans, P.B., Garing, J., 1983. The Snake Range d'ecollement: an exhumed mid-Tertiary ductile-brittle transition. Tectonics 2, 239–263.
- Miller, E.L., Gans, P.B., Wright, J.E., Sutter, J.F., 1988. Metamorphic history of the east central Basin and Range Province: tectonic setting and relationship to magmatism. In: Ernst, W.G. (Ed.), Metamorphism and Crustal Evolution, Western United States: Englewood Cliffs. Prentice-Hall, New Jersey, Rubey Volume VII, pp. 649–682.
- Miller, E.L., Gans, P.B., Grier, S.P., 1994. Geologic Map of the Windy Peak 7.5'Quadrangle, White Pine County, Nevada. USGS Open-File Report OF. -94-687, scale 1:24,000, 1 sheet.
- Miller, E.L., Dumitru, T.A., Brown, R.W., Gans, P.B., 1999A. Rapid Miocene slip on the Snake range–deep Creek range fault system, east-central Nevada. Geol. Soc. Am. Bull. 111, 886–905.
- Miller, E.L., Gans, P.B., Grier, S.P., Huggins, C.C., Lee, J., 1999B. Geologic map of the old man's Canyon quadrangle, Nevada. Nevada Bur. Mines Geol. Field Studies Map 21, 12 scale 1:24,000, 1 sheet.
- Morris, A., Gee, J.S., Pressling, N., John, B.E., MacLeod, C.J., Grimes, C.B., Searle, R.C., 2009. Footwall rotation in an oceanic core complex quantified using reoriented Integrated Ocean Drilling Program core samples. Earth Planet Sci. Lett. 287, 217–228. https://doi.org/10.1016/j.epsl.2009.08.007.
- Nabelek, P.I., Whittington, A.G., Hofmeister, A.M., 2010. Strain heating as a mechanism for partial melting and ultrahigh temperature metamorphism in convergent orogens: implications of temperature-dependent thermal diffusivity and rheology. J. Geophys. Res. 115, 17. https://doi.org/10.1029/2010JB007727. B12417.
- Pavlis, T.L., 1986. The role of strain heating in the evolution of megathrusts. J. Geophys. Res. Solid Earth 91 (12), 407–412. https://doi.org/10.1029/JB091iB12p12407, 422
- Platt, J.P., Behr, W.M., Cooper, F.J., 2015. Metamorphic core complexes: windows into the mechanics and rheology of the crust. J. Geol. Soc. London 172, 9–27. https://doi. org/10.1144/jgs2014-036.
- Poole, F.G., Stewart, J.H., Palmer, A.R., Sandberg, C.A., Madrid, R.J., Ross Jr., R.J., Hintze, L.F., Miller, M.M., Wricke, C.T., 1992. Latest Precambrian to latest Devonian time; development of a continental margin. In: Burchfiel, B.C., Lipman, P.W., Zoback, M.L. (Eds.), The Cordilleran Orogen: Conterminous US: the Geology of North America. G-3. Geol. Soc. Amer, Boulder, Colorado, pp. 9–56. https://doi.org/ 10.1130/DNAG-GNA-G3.9.
- Ramsay, J.G., 1967. Folding and Fracturing of Rocks. McGraw-Hill, New York, p. 560.Ramsay, J.G., Huber, M.I., 1983. Techniques of modern structural geology. Strain Analysis, 1. Academic Press, London, p. 307.
- Rodgers, D.W., 1987. Thermal and Structural Evolution of the Southern Deep Creek Range, West Central Utah and East Central Nevada [Ph.D. Dissertation]. Stanford University, Stanford, California, p. 149, 5 plates.
- Rogowitz, A., White, J.C., Grasemann, B., 2016. Strain localization in ultramylonitic marbles by simultaneous activation of dislocation motion and grain boundary sliding (Syros, Greece). Solid Earth 7, 355–366. https://doi.org/10.5194/se-7-355-2016.
- Singleton, J.S., Mosher, S., 2012. Mylonitization in the lower plate of the Buckskin-Rawhide detachment fault, west-central Arizona: implications for the geometric evolution of metamorphic core complexes. J. Struct. Geol. 39, 180–198. https://doi.org/10.1016/j.jsg.2012.02.013.
- Smith, M.E., Carroll, A.R., Jicha, B.R., Cassel, E.J., Scott, J.J., 2014. Paleogeographic record of Eocene Farallon slab rollback beneath western North America. Geology 42, 1039–1042. https://doi.org/10.1130/G36025.1.
- Snell, K.E., Koch, P.L., Druschke, P., Foreman, B.Z., Eiler, J.M., 2014. High elevation of the 'nevadaplano' during the late cretaceous. Earth Planet Sci. Lett. 386, 52–63. https://doi.org/10.1016/j.epsl.2013.10.046.
- Sonder, L.J., Jones, C.H., 1999. Western United States extension: how the west was widened. Annu. Rev. Earth Planet Sci. 27, 417–462. https://doi.org/10.1146/ annurev.earth.27.1.417.
- Stewart, J.H., 1980. Geology of Nevada: a discussion to accompany the geologic map of Nevada. Nevada Bur. Mines Geol. Spec. Publ. 4, 136.
- Stipp, M., Stunitz, H., Heilbronner, R., Schmid, S.M., 2002. The eastern Tonale fault zone: a 'natural laboratory' for crystal plastic deformation over a temperature range from 250° to 700° C. J. Struct. Geol. 24, 1861–1884.

- Stockli, D.F., 1999. Regional Timing and Spatial Distribution of Miocene Extension in the Northern Basin and Range Province [Ph.D. Dissertation]. report. Stanford University, Palo Alto, California, p. 239.
- Taylor, W.J., Bartley, J.M., Lux, D.R., Axen, G.J., 1989. Timing of Tertiary extension in the Railroad Valley-Pioche transect, Nevada: constraints from ⁴⁰Ar/³⁹Ar ages of volcanic rocks. J. Geophys. Res. 94, 7757–7774. https://doi.org/10.1029/ IB004JB06s07757
- Taylor, W.J., Bartley, J.M., Martin, M.W., Geissman, J.W., Walker, J.D., Armstrong, P.A., Fryxell, J.E., 2000. Relations between hinterland and foreland shortening: Sevier orogeny, central North American Cordillera. Tectonics 19 (6), 1124–1143. https://doi.org/10.1029/1999TC001141.
- Wells, M.L., Allmendinger, R.W., 1990. An early history of pure shear in the upper plate of the Raft River metamorphic core complex: black Pine Mountains, southern Idaho. J. Struct. Geol. 12 (7), 851–867.
- Wernicke, B., 1981. Low-angle normal faults in the Basin and Range Province: nappe tectonics in an extending orogen. Nature 291, 645–648. https://doi.org/10.1038/ 291645a0.
- Wernicke, B., Burchfiel, B.C., 1982. Modes of extensional tectonics. J. Struct. Geol. 4, 105–115. https://doi.org/10.1016/0191-8141(82)90021-9.
- Whitebread, D.H., 1969. Geologic map of the wheeler peak and garrison quadrangles, Nevada and Utah, 1:48,000, 1 sheet USGS Misc. Geol. Invest. Map I-578, scale.
- Whitney, D.L., Teyssier, C., Rey, P., Buck, R.W., 2013. Continental and oceanic core complexes. Geol. Soc. Am. Bull. 125, 273–298. https://doi.org/10.1130/B30754.1.
- Womer, J.B., Thesis], N.V.[M.S., 2017. Late Mesozoic shortening structures in the western portion of the northern Snake Range metamorphic core complex. In: White Pine County. University of California, Santa Barbara, p. 47.

- Wrobel, A.J., 2020. Exploring the Tectonic and Thermal Evolution of the Northern Snake Range Metamorphic Core Complex: Insights from Field Study and Potassium Feldspar ⁴⁰Ar/³⁹Ar Thermochronology [Ph.D. Dissertation]. report. University of California, Santa Barbara, p. 117.
- Wrobel, A.J., Gans, P.B., Womer, J.B., 2021. Late Cretaceous crustal shortening in the Northern Snake Range metamorphic core complex: constraints on the structural geometry and magnitude of pre-extensional footwall burial. Tectonics 40, e2020TC006460. https://doi.org/10.1029/2020TC006460.
- Yonkee, W.A., Weil, A.B., 2015. Tectonic evolution of the sevier and Laramide belts within the North American cordillera orogenic system. Earth Sci. Rev. 150, 531–593. https://doi.org/10.1016/j.earscirev.2015.08.001.
- Yonkee, W.A., Dehler, C.D., Link, K., Balgord, E.A., Keeley, J.A., Hayes, D.S., Fanning, C. M., Wells, M.L., Johnston, S.M., 2014. Tectono-stratigraphic framework of Neoproterozoic to Cambrian strata, west-central U.S.: protracted rifting, glaciation, and evolution of the North American Cordilleran margin. Earth Sci. Rev. 136, 59–95.
- Young, J.C., 1960. Structure and Stratigraphy in the North-Central Schell Creek Range, Eastern Nevada [Ph.D. Dissertation]. report. Princeton University, Princeton, New Jersey, p. 207 (3 plates).
- Zuza, A.V., Thorman, C., Henry, C., Levy, D., Dee, S., Long, S., Sandberg, C., Soignard, E., 2020. Pulsed Mesozoic Deformation in the Cordilleran Hinterland and Evolution of the Nevadaplano: Insights from the Pequop Mountains, Northeast Nevada. Lithosphere, pp. 1–24. https://doi.org/10.2113/2020/8850336, 2020.
- Zuza, A.V., Levy, D.A., Mulligan, S., 2022. Geologic field evidence for non-lithostatic overpressure recorded in the North American Cordillera hinterland, northeast Nevada. Geosci. Front. 13, 101099 https://doi.org/10.1016/j.gsf.2020.10.006.